To the Graduate Council:

I am submitting herewith a thesis written by Miroslaw M. Bialkowski entitled "Study of Charge Emission from Si and Ge Irradiated by a KrF Excimer Laser." I have examined the final copy of this thesis for form and content and recommend that it be accepted in partial fulfillment of the requirements for the degree of Master of Science, with the major in Physics.

T. A. Callcott

Thomas A. Callcott, Major Professor

We have read this thesis

and recommend its acceptance:

G. S. Hurst

D. H. Lowndes

Vasilios Kleanides

James E. Parks

Accepted for the Council:

Carolyn Minkel

Vice Provost
and Dean of The Graduate School

STATEMENT OF PERMISSION TO USE

In presenting this thesis in partial fulfillment of the requirements for a Master's degree at The University of Tennessee, Knoxville, I agree that the Library shall make it available to borrowers under rules of the Library. Brief quotations from this thesis are allowable without special permission, provided that accurate acknowledgment of the source is made.

Permission for extensive quotation from or reproduction of this thesis may be granted by my major professor, or in his absence, by the Head of Interlibrary Services when, in the opinion of either, the proposed use of the material is for scholarly purposes. Any copying or use of the material in this thesis for financial gain shall not be allowed without my written permission.

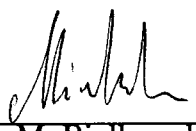

Miroslaw M. Bialkowski

Date: April 11, 1989

STUDY OF CHARGE EMISSION FROM Si AND Ge IRRADIATED BY A KrF EXCIMER LASER

A Thesis

Presented for the

Master of Science

Degree

The University of Tennessee, Knoxville

Miroslaw M. Bialkowski

May 1989

ACKNOWLEDGMENTS

I would like to express my sincere gratitude to Dr. G. Samuel Hurst for his guidance in Resonance Ionization Spectroscopy and Atom Counting; to Dr. Douglas H. Lowndes and Dr. James E. Parks for their help in collecting the experimental data and to Dr. Thomas A. Callcott, Dr. John O. Thomson, and Dr. Vasilios Alexiades for their assistance and valuable discussions.

I would also like to thank Dr. James E. Parks and Dr. William Gibson for creating the environment which enabled me to complete this project, and Ms. Shannon Bays for her assistance in the preparation of this thesis.

ABSTRACT

We described an experiment that was a part of the development of an improved method for counting noble gas atoms (the RISTRON project). Its main purpose was to investigate the charge emission from Si and Ge surfaces under KrF excimer laser irradiation. We proved that this charge should not interfere with functioning of the ion optics associated with the RISTRON, which requires the combination of RIS with a mass selector.

Experimental data were presented in a form of emission signals and compared to the results of theoretical calculations based on a simple mathematical model. We observed unexpected differences between emission signals from Si and Ge. The significance of this discovery justifies continued experimental and theoretical work on the annealing of semiconducting materials.

TABLE OF CONTENTS

CHAPTER			PAGE
1.	Introduction		1
2.	Theory		6
	A.	Introduction	6
	B.	Behavior of a free charge in an electrostatic field	6
	C.	Effects related to charge emission during pulsed laser annealing	16
3.	Experimental setup and initial measurements		20
4.	Experimental results on KrF laser induced charge emission from Si and Ge surfaces		27
	A.	Introduction	27
	B.	Data below the melting threshold	28
	C.	Data above the melting threshold	33
5.	Discussion		44
6.	Conclusions		61
References			63
Appendix A:	Electrical potential W and field F distribution in a conducting cylindrical box		67
Appendix B:	Potential W distribution in a cylindrical box obtained by numerical program FIELD		77
Appendix C:	Sample results of trajectory calculations by program TRAJS for charged particles emitted into the accelerating field F in direction of force		81
Appendix D:	Sample results of analytical calculations of the final time of flight for charges accelerated in a uniform electrostatic field		85
Appendix E:	Sample results of trajectory calculations by program TRAJS for charged particles emitted into the electrostatic field F against the force		88
Vitae			92

LIST OF TABLES

TABLE		PAGE
1.	Chemical and electronic properties of Si and Ge	4
2.	Comparison of analytical calculations of the time of flight of an electron in a uniform electrostatic field with the collection time in a real field calculated numerically for the geometry of our experimental setup	11
3.	Comparison of analytical calculations of the time of flight of Si^+ ions in a uniform electrostatic field with the collection time in a real field calculated numerically for the geometry used in our experiment	12
4.	Comparison of analytical calculations of the time of flight of Ge^+ ions in a uniform electrostatic field with the collection time in a real field calculated numerically for the geometry used in our experiment	13
5.	Behavior of e^-, Si^+, Ge^+ in a reversed electrostatic field for a bias voltage of 1500 volts; t_o and V_o were obtained analytically with the use of eqs. (9) and (10); $r_f - r_i$ and t_o (TRAJS) were obtained numerically by the program TRAJS (Appendix E)	15

LIST OF FIGURES

FIGURE		PAGE
1.	The RISTRON schematic	2
2.	Schematic of the charge collecting setup	8
3.	Experimental setup at IRIS	21
4.	Signals recorded during the charge emission from Al; a) Ch 1 - negative charge emission signal, b) Ch 2 - N_2 laser pulse, c) RF 1 - background noise.	23
5.	Signal of the charge emitted from Al biased by a negative voltage V_1 after subtracting the background noise	24
6.	Maximum of the emission signal and the number of electrons emitted from Al as a function of applied negative bias voltage..	25
7.	Experimental setup at ORNL	26
8.	Original pictures of: a) KrF excimer laser pulse, b) reflectivity of Si when melted by the KrF laser pulse	29
9.	Emission signals for germanium targets below the melting threshold with a negative bias voltage; a) KrF excimer laser signal, b) emission signal for E = .25 J/cm^2, V_1 = -1000 V, c) emission signal for E = .25 J/cm^2, V_1 = -1500 V.	30
10.	Emission signals for silicon targets below the melting threshold with a negative bias voltage; a) KrF excimer laser signal, b) emission signal for E = .9 J/cm^2, V_1 = -500 V, c) emission signal for E = .9 J/cm^2, V_1 = -1000 V, d) emission signal for E = .9 J/cm^2, V_1 = -1500 V.	31
11.	Emission signals for germanium targets below the melting threshold with a positive bias voltage; a) KrF excimer laser signal, b) emission signal for E = .25 J/cm^2, V_1 = +500 V, c) emission signal for E = .25 J/cm^2, V_1 = +1000 V.	32

FIGURE PAGE

12. Emission signals for silicon targets below the melting threshold with a positive bias voltage;
a) emission signal for E = .9 J/cm^2, V_1 = +500 V,
b) emission signal for E = .9 J/cm^2, V_1 = +1000 V,
c) emission signal for E = .9 J/cm^2, V_1 = +1500 V,
d) emission signal for E = .9 J/cm^2, V_1 = +2000 V,
e) KrF excimer laser signal. 34

13. Emission signals for germanium targets above the melting threshold with positive and negative bias voltages;
a) KrF excimer laser signal,
b) emission signal for E = .6 J/cm^2, V_1 = +1000 V,
c) emission signal for E = .35 J/cm^2, V_1 = -500 V,
d) emission signal for E = .6 J/cm^2, V_1 = -500 V. 35

14. Emission signals for silicon targets above the melting threshold with a negative bias voltage;
a) KrF excimer laser signal,
b) emission signal for E = 1.25 J/cm^2, V_1 = -500 V,
c) emission signal for E = 1.50 J/cm^2, V_1 = -500 V. 36

15. Maxima of the charge emission signals from silicon as a function of applied negative bias voltage;
a) E = .9 J/cm^2,
b) E = 1.25 J/cm^2,
c) E = 1.50 J/cm^2. 38

16. Maxima of the charge emission signals from germanium as a function of applied negative bias voltage;
a) E = .25 J/cm^2,
b) E = .35 J/cm^2,
c) E = .60 J/cm^2. 39

17. Total time of charge emission for silicon at a negative bias voltage;
a) E = .9 J/cm^2,
b) E = 1.25 J/cm^2,
c) E = 1.50 J/cm^2. 40

18. Total time of charge emission for germanium at a negative bias voltage;
a) E = .25 J/cm^2,
b) E = .35 J/cm^2,
c) E = .60 J/cm^2. 41

FIGURE PAGE

19. Maxima of the charge emission signals from germanium as a function of applied positive bias voltage;
a) $E = .25\ J/cm^2$,
b) $E = .60\ J/cm^2$. 42

20. Maxima of the charge emission signals from silicon as a function of applied positive bias voltage;
a) $E = .9\ J/cm^2$,
b) $E = 1.25\ J/cm^2$,
c) $E = 1.50\ J/cm^2$. 43

21. Time of flight of electrons accelerated in a uniform electrostatic field calculated analytically for different initial velocities and bias voltages;
a) $v_o = .6 \cdot 10^7$ m/s,
b) $v_o = 10$ m/s. 46

22. Time of flight of Si^+ ions accelerated in a uniform electrostatic field calculated analytically for different initial velocities and bias voltages;
a) $v_o = 4 \cdot 10^4$ m/s,
b) $v_o = 10$ m/s. 47

23. Time of flight of Ge^+ ions accelerated in a uniform electrostatic field calculated analytically for different initial velocities and bias voltages;
a) $v_o = 4 \cdot 10^4$ m/s,
b) $v_o = 10$ m/s. 48

24. Original emission signals $V_c(t)$ from the solid (unmelted) Ge and Si surfaces biased by a negative voltage V_1, irradiated by KrF laser pulse of energy density $E = 250\ mJ/cm^2$ for Ge, and $E = 900\ mJ/cm^2$ for Si. 50

25. Original emission signals $V_c(t)$ from Ge and Si surfaces biased by a negative voltage V_1, irradiated by a KrF laser pulse of energy density $E = 350\ mJ/cm^2$ for Ge and $E = 1 J/cm^2$ for Si 51

26. Original emission signals $V_c(t)$ from Ge and Si surfaces biased by a negative voltage V_1 irradiated by a KrF laser pulse of energy density $E = 600\ mJ/cm^2$ for Ge and $E = 1.5 J/cm^2$ for Si. 52

27. Original emission signals $V_c(t)$ from Ge and Si surfaces biased by positive voltage $V_1 = +1000$ V, irradiated by KrF laser pulses of different energy densities E. 53

FIGURE PAGE

28. Number of electrons emitted from Ge at negative bias voltages;
a) E = .25 J/cm^2,
b) E = .35 J/cm^2,
c) E = .50 J/cm^2,
d) E = .60 J/cm^2. 55

29. Number of electrons emitted from Si at negative bias voltages;
a) E = 0.90 J/cm^2,
b) E = 1.0 J/cm^2,
c) E = 1.25 J/cm^2,
d) E = 1.5 J/cm^2. 56

30. Number of ions emitted from Ge at positive bias voltages;
a) E = .25 J/cm^2,
b) E = .60 J/cm^2. 57

31. Number of ions emitted from Si at positive bias voltages;
E = .90 J/cm^2. 58

32. Number of electrons emitted from Ge and Si versus KrF laser energy density on a log-log scale;
Ge: a) V_1 = -500 V, b) V_1 = -1000 V, c) V_1 = -2000 V,
Si: a) V_1 = -100 V, b) V_1 = -250 V, c) V_1 = -500 V,
d) V_1 = -1000 V, e) V_1 = -1500 V. 59

LIST OF SYMBOLS

SYMBOL	DEFINITION	FIRST PAGE
α	angle between initial velocity and field vectors	11
λ	electromagnetic wave length	4
a	acceleration of a charged particle in the field	9
$2a_i$	i-th root of Bessel function of the zero-th order	67
A	atomic weight	1
A_i	first coefficient of the i-th term in the potential solution	67
B_i	second coefficient of the i-th term in the potential solution	67
C	total capacitance of the input circuit	7
e	elementary charge; $e = 1.6 \cdot 10^{-19}$ C	7
E	KrF laser energy density	28
F	electrostatic field	6
h	distance target - collector; h = 15 mm	7
j_e	total emission current density	16
j_k	k-photon photoemission current density; k > 0	16
j_o	thermionic emission current density	16
J_e	total emission current	27
$J_{e/max}$	maximum value of the total emission current	38
K_o	initial kinetic energy of a particle	10
m	mass of a particle; m(e-) = 0.000549 a.m.u., m(Si+) = 28.086 a.m.u., m(Ge+) = 72.5899 a.m.u	9
n	number of terms in the potential solution	67
N	number of charged particles	7
q	total charge collected	27
r	distance from the axis of symmetry	67

SYMBOL	DEFINITION	FIRST PAGE
r_f	final radial position of particle trajectory	15
r_i	initial radial position of particle trajectory	11
R	input resistance	8
t	total time of flight of charged particles in the experiment (length of the emission signal)	9
t_f	time of flight of charged particles calculated analytically	6
t_o	time for particles to lose their initial velocity in the field	10
t_R	relaxation time of electron-lattice system	16
T_e	electron temperature	18
T_L	lattice temperature	18
T_m	melting point	4
U_c	energy of the field used in transportation of charged particles	7
U	total initial energy of the field	7
v	velocity of charged particles	9
v_o	initial velocity of charged particles	9
V	target- collector instant voltage	7
V_o	maximum value of the signal in a reversed field	10
V_1	target bias voltage	6
V_c	pulsed voltage recorded by the collector	7
V_f	maximum of the signal recorded by the collector	10
W	electrostatic potential	6
x	position of an ion w.r.t. the collector	7
z	position of an ion w.r.t. the target	67
Z	atomic number	1

CHAPTER 1

INTRODUCTION

In recent years there has been a lot of interest in single atom counting in many branches of science including physics, geology and cosmology. After a device called the Maxwell demon was proven successful [1] another idea for a better detector and counter called the RISTRON (Fig.1) was proposed and subsequently discussed [2-4].

The main concept of the RISTRON (see Fig.1) is based on a combination of the Resonance Ionization Spectroscopy (RIS), Mass Spectroscopy and single atom detection. The RIS process allows one to select atoms by their atomic number Z, and a mass spectrometer selects atoms by their atomic weight A. As a result ions of specific atoms (A,Z) can be directed into a semiconductor solid wafer, called the "atom bank," and stored. During their implantation secondary electron emission from the target takes place and can be used for counting the number of implanted ions.

Because of limited abundance sensitivity of mass filters we have to repeat the whole cycle several times in order to reduce the background due to adjacent masses. Automatic recirculation of the entire population of the atoms takes place between two targets in an actively pumped vacuum system. In order to recover desired species of atoms from the target we melt its surface with an excimer laser pulse. As soon as the rapid melting is over, the liquid-solid interface starts to propagate back. If our atoms of interest (possibly Kr) are more soluble in the liquid target material (possibly Si or Ge) processes of separation

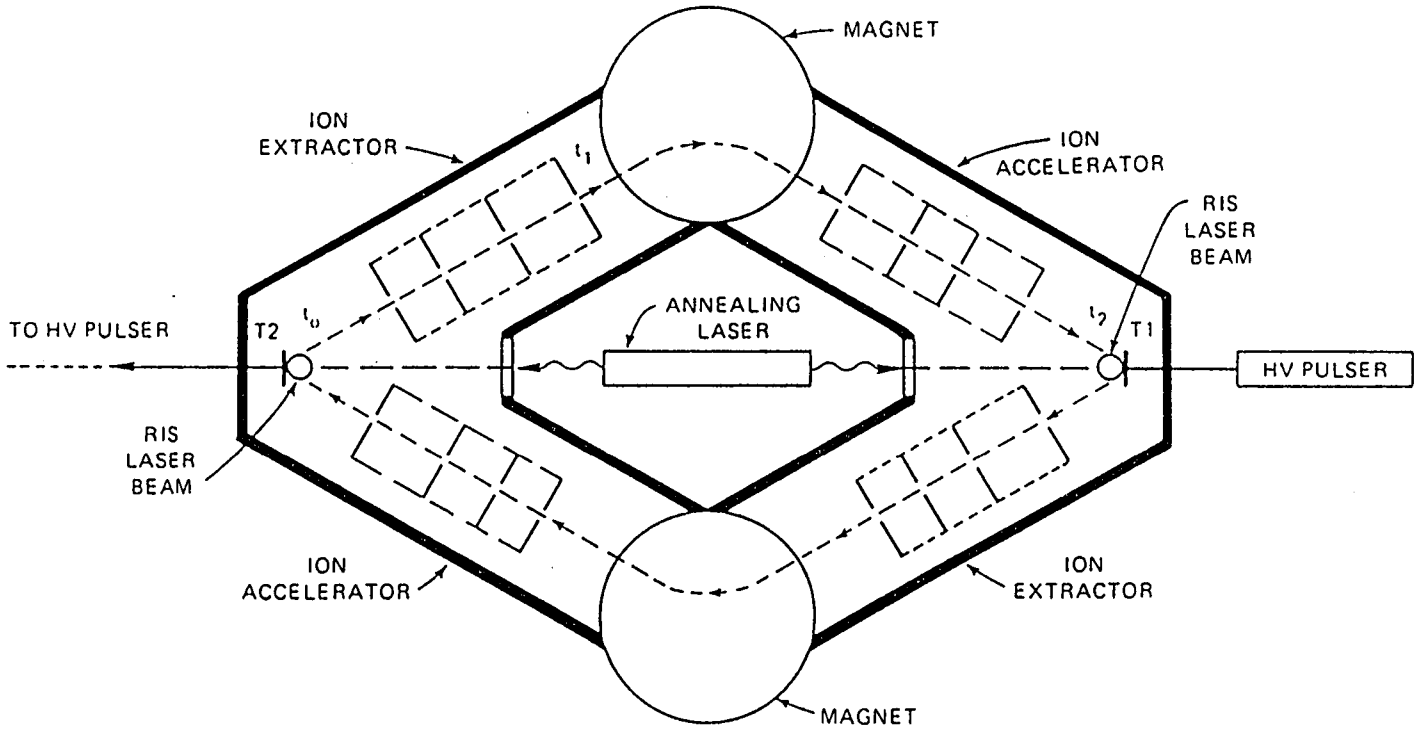

Fig.1: The RISTRON schematic.

and segregation to the surface take place. We expect that in the RISTRON all of them will be expelled to the gas phase.

During the laser irradiation, processes of material vaporization and charge emission from the target occur. That raises a question whether or not the space charge or plasma effects on the surface would complicate the ion optics required to transport ions between a pair of targets.

Pellissippi International Inc. and The University of Tennessee Institute of Resonance Ionization Spectroscopy (IRIS) undertook research to answer this question with the support of an NSF Phase I SBIR grant. This thesis is derived in large part from these studies.

The initial part of the project was carried out at IRIS and included design and construction of the experimental setup and verification of the technique of measurement. Data were taken from a sample of aluminum irradiated with pulses from a 337.1 nm nitrogen laser.

The main part of the experiment was performed at the Oak Ridge National Laboratory, Solid State Division, where more precise data were obtained. In this case silicon and germanium materials were used as the targets, and 248 nm light from the KrF excimer laser was used as a source of irradiation.

The applied portion of the project has been successfully completed. A lot of very good data has been collected and the initial question is answered satisfactorily by demonstrating that space charge effects will not affect ion transport [5,6].

While studying the problem of charge emission from materials irradiated with short (nanosecond) excimer laser pulses, we noticed that some of our data were more complicated than we expected. Although Si and Ge have similar chemical and electronic properties (Table 1), some of their charge emission

TABLE 1

Chemical and electronic properties of Si and Ge

Property [unit]		Si	Ge
Absorption coeff. [cm^{-1}] at 300 K		$4.5 \cdot 10^3$	$5.0 \cdot 10^5$
at Tm		$2.2 \cdot 10^5$	$7.0 \cdot 10^5$
Atomic number		14	32
Atomic weight		28.09	72.59
Boiling point [C]		2355	2830
Density of liquid [g/cm^3]		2.5	5.5
Density of solid [g/cm^3] at 300 K		2.33	5.32
Electron work function [eV]			
photoelectric		4.37-4.67	4.3-4.8
thermionic		3.54-4.02	---
Energy gap at 300 K [eV]		1.12	0.67
Energy of the major Auger lines [eV]	I	91	24
	II	1610	44
Heat of fusion [kJ/mol]		50.2	31.8
Heat of vaporization [kJ/mol]		359.0	334.3
Ionization potential [V]	I	8.15	7.88
	II	16.34	15.93
	III	33.49	34.21
Lattice parameter at room temp. [Å]		5.43	5.66
Melting point [C]		1410	937
Mobility of electrons [$cm^2/V/sec$]		1350	3900
Mobility of holes [$cm^2/V/sec$]		480	1900
Molar heat capacity [J/mol/k] at 273.2K		20.0	23.3
Reflectivity for λ= 6328 Å at 300 K		.35	.49
at Tm		.42	.51
Reflectivity for λ= 2480 Å at 300 K		.66	.65
at Tm		.63	.55
for liquid		.70	.65
Resistivity at 273.2 K [$\Omega \cdot m$]		0.1-60.0	0.001-0.5
Specific gravity at 300 K		2.33	5.323
Specific heat at 300 K [cal/g/K]		0.168	0.077
Thermal conductivity at 300 K [W/m/k]		165	67
Thermal diffusivity [cm^2/s] at 300 K		1.35	0.35
at Tm		0.196	0.075
Vapor pressure at Tm [torr]		$1.0 \cdot 10^{-3}$	$7.0 \cdot 10^{-7}$
Vaporization point [K]		2750	2980

characteristics are very different and raise interesting fundamental question about the emission process.

The most puzzling is the difference between Si and Ge emission currents, particularly when the samples are biased by a positive voltage. Moreover, the charge emission from Ge does not agree with any earlier observations for a positive charge. The unexpectedly short emission signals indicate that processes standing behind this phenomenon are not very well known and require more detailed experiments.

This thesis presents the results of an experimental investigation of charge emission from Ge and Si with respect to the RISTRON project, and also initiates a discussion on the effects related to charge emission following a short pulse laser irradiation of semiconducting materials.

CHAPTER 2

THEORY

A. INTRODUCTION

Before getting into details of experimental procedures and the results of measurements, we describe a simple model of electron (and singly charged ion) behavior in an electrostatic field and briefly summarize effects related to the charge emission following irradiation of semiconducting surfaces by the KrF excimer laser. The model of electron motion is a good approximation to the geometry and the experimental conditions. The results of our calculations are followed by corresponding experimental data.

The most important features of this model are the potential W, the field distribution between the target and the collector F, and the time (t_f) it takes for Si^+, Ge^+ or e^- to travel this distance. These calculations provide a means of calculating the lifetime of the space charge created by the laser annealing and indicate what parameters of the experiment (mainly bias voltage V_1) it depends on.

B. BEHAVIOR OF A FREE CHARGE IN AN ELECTROSTATIC FIELD.

The motion of a charged particle in an electrostatic field depends on three factors:

a) shape of lines of force,

b) initial state of the particle (position, velocity, etc.),

c) presence of other objects (atoms, electrons, ions, etc.).

As a first approximation, we consider the problem of motion of one electron ion in a vacuum (i.e. no other objects around and no interaction except field-ion in a uniform electrostatic field).

In our experiment the field between the electrodes has cylindrical symmetry and is not exactly uniform. Nevertheless, we will assume that the field is approximately uniform in the vicinity of the axis of symmetry. This assumption has been confirmed by an analytic calculation of the electrostatic potential and field inside a cylindrical box with the geometry of our experiment. The calculations and results are presented in Appendix A. This analytic solution has been verified by another program (called FIELD) using numerical methods in Appendix B. Results of the numerical solution will be used for calculations of trajectories.

The experimental geometry is shown schematically in Fig.2. We maintain constant voltage V_1 on the target electrode. Assume the collector electrode to be electrically isolated because it is connected to the ground through a large resistor. The total energy of the target-collector system [7] is $U = 1/2\, C\, V_1^2$ where C is the capacitance of the input circuit. If there are N ions in our system, the electrostatic forces of the field act on them, corresponding charges are induced in the electrodes, and a voltage pulse V_c will appear on the collector plate. When these ions move from h to x the field does the work:

$$U_c = \int_h^x N\, e\, F\, dx' \qquad (1)$$

and the energy of the system will be:

$$\frac{1}{2} C V^2 = \frac{1}{2} C V_1^2 - \int_h^x N\, e\, F\, dx' \qquad (2)$$

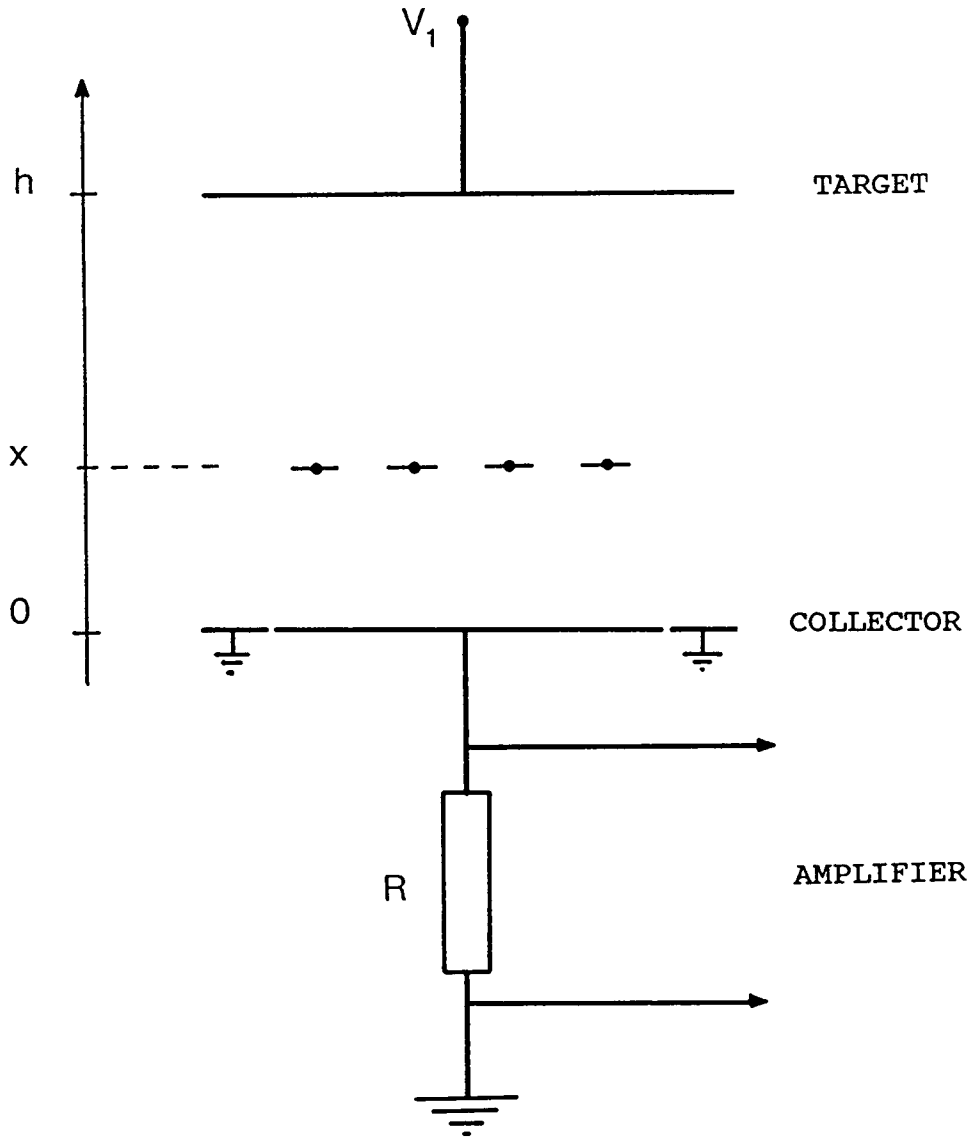

Fig.2: Schematic of the charge collecting setup.

where V is the new potential between the electrodes.

The voltage pulse for $V_c << V_1$ that appears on the collector is:

$$V_c = V_1 - V = \frac{1}{C V_1} \int_h^x N e F \, dx' \qquad (3)$$

If we assume F to be constant

$$V_c = \frac{N e F}{C V_1} \int_h^x dx' = \frac{N e}{C V_1} (x - h) \qquad (4)$$

For $F = \frac{V_1}{h}$ and $x(t) = h - v t$

$$V_c = - \frac{N e}{C h} \int_o^t v \, dt' \qquad (5)$$

The time of collection t_f can be introduced through

$$h = v_o t_f + \frac{1}{2} a t_f^2, \quad \text{as} \quad t_f = \frac{\sqrt{(v_o^2 + 2 a h)} - v_o}{a}$$

where v_o is the initial velocity.

If we take: $a = \frac{e V_1}{m h}$

$$t_f = \frac{m h v_o}{e V_1} \left(\sqrt{\left(\frac{2 e V_1}{m v_o} + 1 \right)} - 1 \right) \qquad (6)$$

$v = v_o + a t$ substituted in (5) gives:

$$- V_c = \frac{N e v_o}{C h} t + \frac{N e F}{2 C h m} t^2 \qquad (7)$$

For $t = t_f$ we get the final value of V_c as:

$$-V_f = \frac{N e}{C} \qquad (8)$$

If we reverse direction of the field F, only the ions with nonzero initial velocity v_o get into the space between the target and the collector. They will be slowed down, and if they stop before reaching the collector, they will be accelerated back to the target electrode. In this case the total time of flight is

$$t_f = 2 t_o = \frac{2 v_o}{a} = \frac{2 m h v_o}{e V_1} \qquad (9)$$

and the maximum of the obtained signal is

$$-V_o = \frac{N m v_o}{2 C V_1} = \frac{N K_o}{C V_1} \qquad (10)$$

where K_o is the initial kinetic energy.

For the above model we simulate emission of ions into a uniform electrostatic field. In order to calculate the time of their flight between a target and a collector, we use the eq. (6). For the real field, calculated numerically in Appendix B, we emit ions from two different initial positions of the target at three initial angles with respect to the axis of symmetry of the cylinder. Tables 2-4 show the results of the analytical calculations and compare them with the results obtained by the program TRAJS in Appendix C. These calculations give an estimate of the lifetime of a created space charge if its only interaction is with the field.

TABLE 2

Comparison of analytical calculations of the time of flight of an electron in a uniform electrostatic field with the collection time in a real field calculated numerically for the geometry of our experimental setup.

K_o	v_o	t_f	Final Time by TRAJS [ns]					
			r_i = .5mm			r_i = 5.0 mm		
[eV]	[m/s]	[ns]	$\alpha=0$	$\alpha=.5$	$\alpha=1$	$\alpha=0$	$\alpha=.5$	$\alpha=1$
0.001	1.9 E4	1.3	1.2	1.2	1.2	1.2	1.2	1.2
1.0	5.9 E5	1.3	1.2	1.2	1.2	1.2	1.2	1.2
2.0	8.4 E5	1.3	1.2	1.2	1.2	1.2	1.2	1.2
3.0	1.0 E6	1.3	1.2	1.2	1.2	1.2	1.2	1.2
4.0	1.2 E6	1.2	1.2	1.2	1.2	1.2	1.2	1.2
5.0	1.3 E6	1.2	1.2	1.2	1.2	1.2	1.2	1.2
6.0	1.5 E6	1.2	1.2	1.2	1.2	1.2	1.2	1.2
7.0	1.6 E6	1.2	1.2	1.2	1.2	1.2	1.2	1.2
8.0	1.7 E6	1.2	1.2	1.2	1.2	1.1	1.2	1.2
9.0	1.8 E6	1.2	1.2	1.2	1.2	1.1	1.2	1.2

V_1 = -1500 volts

TABLE 3

Comparison of analytical calculations of the time of flight of Si^+ ions in a uniform electrostatic field with the collection time in a real field calculated numerically for the geometry used in our experiment.

K_o	v_o	t_f	Final Time by TRAJS [ns]					
			r_i = .5mm			r_i = 5.0 mm		
[eV]	[m/s]	[ns]	$\alpha=0$	$\alpha=.5$	$\alpha=1$	$\alpha=0$	$\alpha=.5$	$\alpha=1$
0.001	8.3 E1	296	281	281	281	278	278	278
1.0	2.6 E3	289	276	276	278	271	271	273
2.0	3.7 E3	286	273	273	275	268	271	273
3.0	4.5 E3	284	271	271	276	266	263	271
4.0	5.2 E3	282	268	271	273	266	266	271
5.0	5.9 E3	280	266	268	273	264	266	268
6.0	6.4 E3	278	266	268	273	261	264	268
7.0	6.9 E3	277	264	266	273	261	264	268
8.0	7.4 E3	276	264	266	271	259	261	268
9.0	7.9 E3	275	261	264	271	259	261	266

V_1 = +1500 volts

TABLE 4

Comparison of analytical calculations of the time of flight of Ge^+ ions in a uniform electrostatic field with the collection time in a real field calculated numerically for the geometry used in our experiment.

K_o	v_o	t_f	Final Time by TRAJS [ns]					
			r_i = .5mm			r_i = 5.0 mm		
[eV]	[m/s]	[ns]	$\alpha=0$	$\alpha=.5$	$\alpha=1$	$\alpha=0$	$\alpha=.5$	$\alpha=1$
0.001	5.2 E1	476	451	451	451	447	447	447
1.0	1.6 E3	465	443	443	447	436	436	440
2.0	2.3 E3	460	440	440	443	432	436	440
3.0	2.8 E3	456	436	436	443	428	432	436
4.0	3.3 E3	453	432	436	440	428	428	436
5.0	3.6 E3	450	426	432	440	424	428	432
6.0	4.0 E3	448	428	432	440	420	424	432
7.0	4.3 E3	445	424	428	440	420	424	432
8.0	4.6 E3	443	424	428	436	416	420	432
9.0	4.9 E3	441	420	424	436	416	420	428

V_1 = +1500 volts

For electrons (Table 2), the time of flight in the electrostatic field produced by the bias voltage V_1 = -1500 volts is equal to t_f = 1.2 ns. This value is not significantly affected by changes in initial energy and initial angle of ejection.

In Tables 3 and 4, results of similar calculations are presented for Si^+ and Ge^+ ions. The much heavier ions have proportionally longer time of flight; t_f = 0.3 μs for Si^+ and t_f = 0.5 μs for Ge· If ions are ejected from the surface with small initial velocities, characteristic of thermal ion emission, the small change of initial velocity or change of ejection direction effect the time of flight by only a few percent.

Electrons and ions, created on the surface of the target, can be injected into the field along the direction of the force vector, and, if they have nonzero initial velocity, they can be also injected against the force. As the simulated data show (Table 5), the effect of the field in slowing them down and returning them to the target has negligible influence on the registered ejection signal.

It is obvious that if a cloud of electrons and positive ions is created on the surface of the target, additional effects may occur, such as:

a) expansion of the charge cloud,

b) recombination of ions with electrons in which neutrals are created,

c) scattering of energetic neutrals with excitation or ionization.

In this study, we did not analyze these effects, assuming that they would not interfere with the RISTRON functioning if the bias voltage removed all the charges created during material annealing in a sufficiently short time.

Later, we will see that it may be very important to learn more about these phenomena in order to understand the process of charge emission.

TABLE 5

Behavior of e^-, Si^+, Ge^+ in a reversed electrostatic field, for a bias voltage of 1500 volts; t_o and V_o were obtained analytically with the use of eqs. (9) and (10), $r_f - r_i$ and t_o (TRAJS) were obtained numerically by the program TRAJS (Appendix E).

K_o	$2t_o$	V_o	TRAJS		Particle
			$r_f - r_i$	$2t_o$	
[eV]	[ns]	[mV]	[mm]	[ns]	
1	0.1	0.04	0.0	0.1	
10	0.2	0.44	0.0	0.1	
450	1.4	20.1	0.1	1.4	e^-
950	2.1	42.2	0.2	2.1	
1450	2.6	64.6	0.3	2.7	
1	15.4	0.04	0.0	30.2	
10	48.6	0.44	0.0	30.2	
450	328.0	20.1	0.1	305.4	Si^+
950	475.0	42.2	0.2	465.4	
1450	586.0	64.6	0.3	600.9	
1	24.7	0.04	0.0	48.5	
10	78.1	0.44	0.0	48.5	
450	530.5	20.1	0.1	490.9	Ge^+
950	759.8	42.2	0.2	748.3	
1450	939.7	64.6	0.3	966.0	

Note, that for more realistic initial energies, 1 - 10 eV, the maximum of the signal V_o is very small and cannot influence our experimental values for V_f. For the same amount of one electron ions ($N = 10^{+8}$) we would get the value of $V_f = 66.7$ mV.

Only for very high initial velocities in a reversed field could the motion of particles have influence on the shapes of emission signals and the values of our experimental data.

C. EFFECTS RELATED TO CHARGE EMISSION DURING PULSED LASER ANNEALING

The effects of laser irradiation on the material depend on properties of the target (reflectivity, density, specific heat, latent heat, temperature of melting, etc.), parameters of the laser beam (wavelength, energy density), and the time of interaction [8-13].

The energy of the electromagnetic field of a beam is absorbed by the electrons first, and then, through relaxation processes ($t_R = 10^{-12}$ sec), transferred to the lattice. Absorption of short pulse laser radiation by semiconductors leads to the creation of nonequilibrium carrier densities and elevated carrier and lattice temperatures [14-17]. Because the band gap of most semiconductors decreases with increasing temperature, the band gap will be lowest near the surface where the temperature is highest, causing plasma confinement [18] near the surface. At the same time the carriers can be driven by temperature gradients in a thermoelectric effect. This effect is generally weaker than the effect related to the band bending [14].

Generally, electron emission effects can be described by the total emission current density j_e composed of partial current densities:

$$j_e = \sum_{i=0}^{\infty} j_i \qquad (11)$$

where: j_o is interpreted as a thermionic emission, and j_k is interpreted as a k-photon photoemission, $k > 0$.

Thermionic emission takes place when the surface of the solid is heated to a sufficiently high temperature. Neutral atoms, electrons and positive ions may be ejected.

The photoelectric effect consists of ejection of electrons from the surface of a solid when electromagnetic radiation is incident upon it. The number of photoelectrons produced per unit time is proportional to the photon flux; thus the photoelectric yield, which is the number of photoelectrons per incident quantum of radiation, is independent of intensity.

The most important factors which determine the photoelectric yield are the nature of the solid, oxidation or contamination of its surface and the frequency of the radiation. Under extremely high laser irradiance, photoemission becomes optical field-emission (optical tunneling) if thermionic emission or optical damage does not set in first. This effect is important only in strong electric fields normal to the surface.

Another important source of electrons is the Auger effect. When the atom is in an excited X-ray level, having had one electron removed from an inner shell by whatever means, it may return to a state of lower energy by ejecting one of it's own electrons in a process that competes with the ordinary quantized emission of radiation. This recombination process reduces the number of ground state free electrons but creates energetic electrons high in the conduction band which can easily leave the solid.

A large number of papers [19-23] on laser annealing use a conventional thermal model which assumes that thermal equilibrium is established between the dense electron-hole plasma and the lattice during the laser pulse. High power laser pulses melt and vaporize the material; they can also remove material

as a result of the thermomechanical effect (shock wave). And if the energy of photons is high enough (UV), photoionization of neutral atoms may occur.

An alternative non-thermal model assumes that the atomic lattice is not in equilibrium with the electron-hole plasma, and that the observed effects (for example electron emission) are plasma dependent [24,25].

The emission of charged particles can provide direct information about electron and lattice temperatures. Thermionic emission is a positive indicator of high electron temperatures T_e, while the evaporation of material from the surface is a positive indicator of high lattice temperatures T_L. In the case of nanosecond or longer pulses, the electron temperature can be only slightly higher than the lattice temperature [14]. In this case, thermionic emission masks the multiphoton photoelectric signal, and other phenomena can be hard to separate from the total signal. For sufficiently high laser fluences, besides electrons we have positive ions, neutral atoms, clusters of ions and even microscopic particles may be emitted [26-31].

Among many experiments investigating emission of charged (and neutral) species from semiconductors and metals, the experiments reported by a group of scientists at Harvard University seem to be the most interesting [32-37]. To separate thermal effects they used very short (picosecond) pulses to illuminate Si and Ge. Changing the laser fluence from a very low value to values about six times higher than the threshold for melting, they defined four regimes of emission phenomena. They also estimated initial ion velocities by measuring the time elapsed from the moment of arrival of the laser pulse on the sample to the moment ions reach the collection electrode. For zero accelerating voltage on the collector, the time of arrival of the peak of the ion signal, at collecting electrode positioned 3 mm away from the silicon surface, ranged from a few tens of

nanoseconds to several microseconds. The ion velocity could be deduced from the temporal position of the peak of the signal.

Malvezzi et al. [38] investigated the dynamics of the electron-hole plasma in silicon and germanium and observed that above a certain value of laser fluence, significant deviations between measured and calculated values of reflectivities and transmissions occurred. Their results indicated a strong increase of the recombination rate as soon as the plasma resonances become comparable with the band gap energy. This suggests that new recombination channels are opened at this well defined laser fluence that strongly affects the subsequent evolution of the electron-hole plasma. The onset of a plasma resonance was observed by monitoring the reflectivity as a function of the laser fluence at a fixed delay after the excitation pulse. Particularly in case of Ge which has a relatively low band gap, strong carrier recombination can occur by plasmon emission and affect the temporal evolution of the carrier density.

CHAPTER 3

EXPERIMENTAL SETUP AND INITIAL MEASUREMENTS

The first part of the experiment was designed only as a test of the apparatus and the technique of measurement. As a source of irradiation we used a nitrogen laser (model LN 1000, PRA Intl.,Inc.) with wavelength = 337.1 nm, pulse width = 600 ps, nominal energy per pulse = 1.2 mJ. The beam was focused with a quartz lens of focal length = 25 cm. A small fraction of it was selected by a glass plate beam - splitter in order to monitor the temporal shape of a laser pulse. The pulse was measured with a fast response photodiode and storage oscilloscope. As a target we used an aluminum plate in the shape of a flat disk biased by a high voltage power supply. Charge was collected by a metal disk surrounded by a grounded guard ring and placed parallel to the target at an approximate distance of 15 mm. The emitter and the collector were mounted inside a vacuum system and oriented so that the laser beam was incident on the target at the 45 deg. angle (Fig.3). The vacuum was on the order of 10^{-6} torr.

The capacitance of the emitter - collector system was measured by a bridge method to be 30 ppf. This value had to be added to the 210 ppf capacitance of the lead-in cable.

After some difficulties with a strong transient signal that dominated our recordings when (and shortly after) the N_2 laser was fired, we were able to record signals that were results of a space charge created by N_2 laser illumination of Al target. Signals obtained during the first part of the experiment were averages of

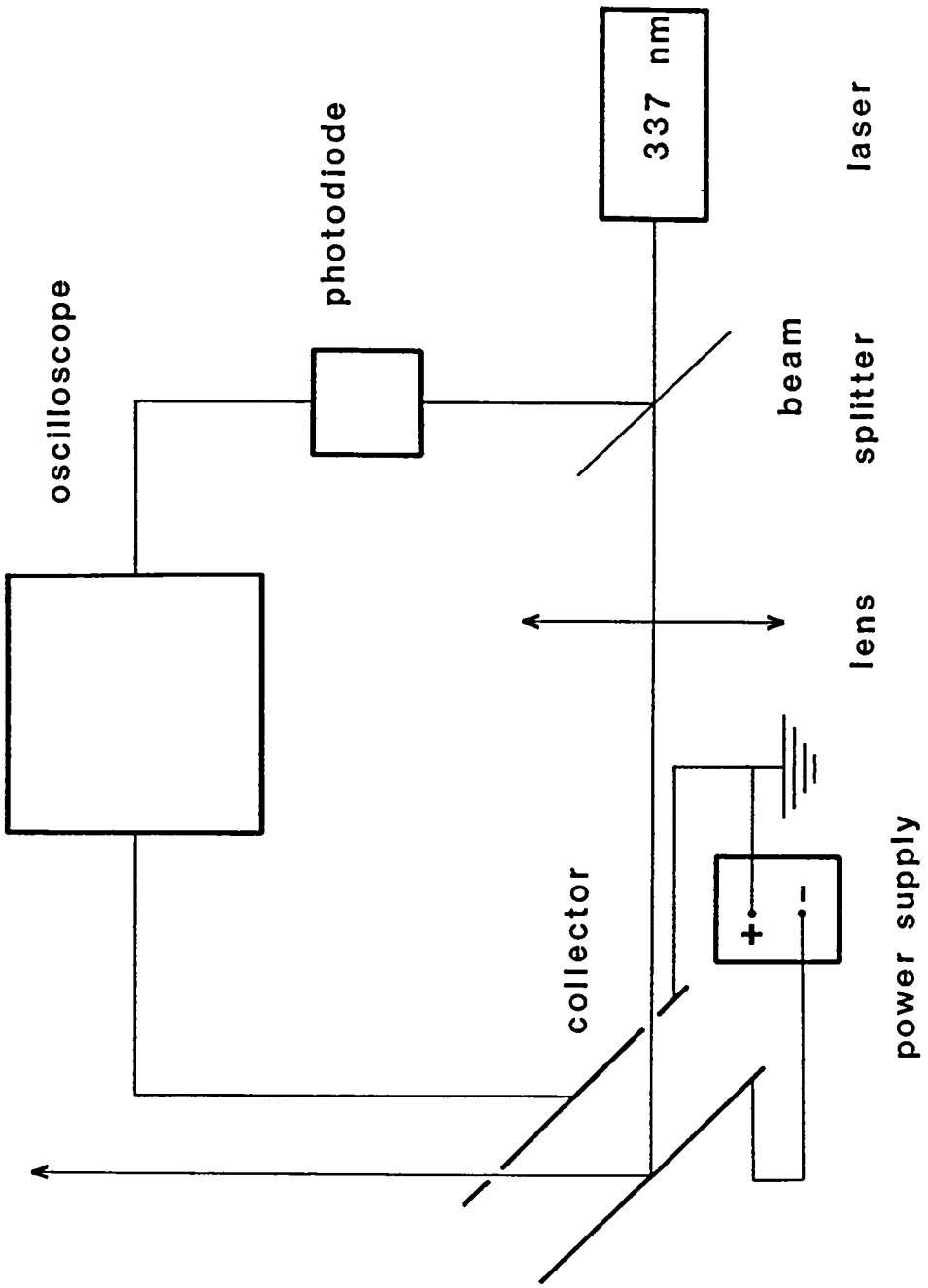

Fig.3: Experimental setup at IRIS.

approximately 100 fast pulses that were electronically recorded, smoothed, averaged, displayed on the screen and plotted (Fig.4).

The transient background signal was a result of a strong discharge between the spark electrodes initiating the lasing process. Thanks to the electronic averaging of many pulses this background was recorded. We could then subtract the transient signal from the total signal to obtain a pulse of the charge emitted from Al as a result of N_2 laser irradiation (Fig.5). Using these graphs and eq. (3) we obtained a function of the number of electrons versus bias voltage applied to the target as shown in Fig. 6.

The second part of the experiment was performed in the Solid State Division at Oak Ridge National Lab. The experimental setup was somewhat modified as shown in Fig. 7. Thin wafers of Si and Ge were used as targets. They rested on a metal plate which could be biased by high positive or negative voltage (V_1). They were irradiated at an angle of 45 deg. with pulses of 248 nm light from a KrF excimer laser (Lambda Physik). The laser produced about 750 mJ pulses; a lens and aperture were used to produce a uniform intensity within a spot several mm in diameter on the targets. The energy densities were adjusted by placing pairs of quartz plates in the laser beam. The emission current as a function of time was measured by a Tektronix 7912 AD Programmable Digitizer and recorded photographically. The laser pulse was similarly recorded. In order to measure the duration of melting in the spot irradiated by the KrF laser, the reflected intensity of a HeNe laser beam was recorded [13].

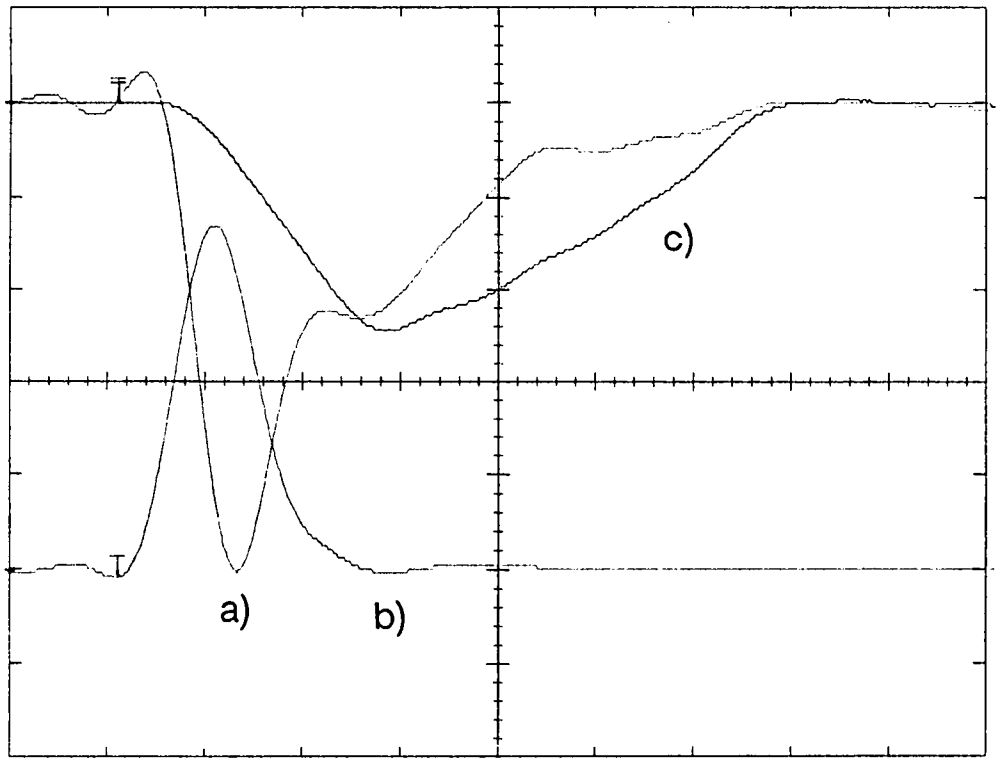

Fig.4: Signals recorded during the charge emission from Al;
a) Ch 1 - negative charge emission signal,
b) Ch 2 - N_2 laser pulse,
c) RF 1 - background noise.

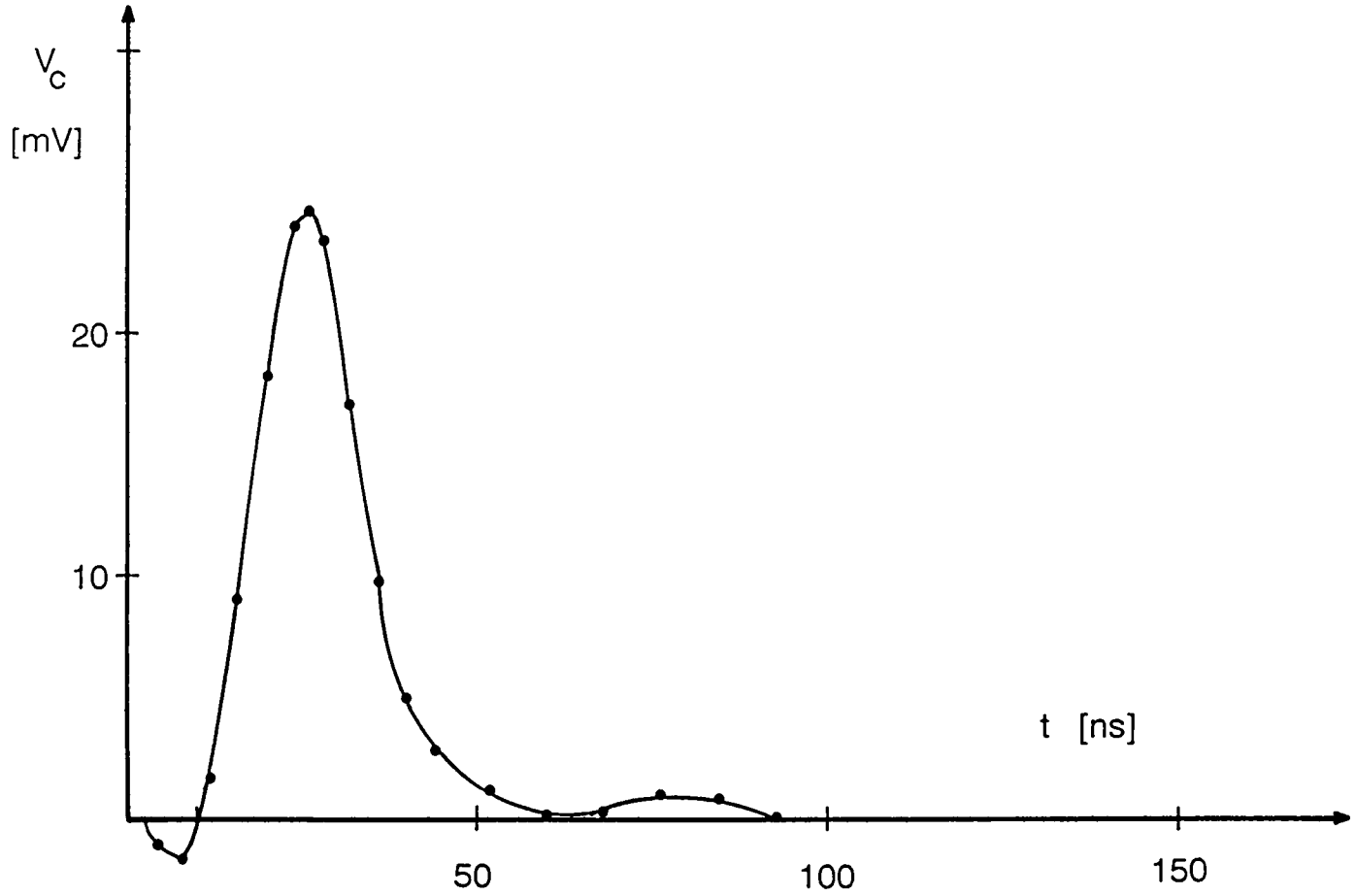

Fig.5: Signal of the charge emitted from Al biased by a negative voltage V_1 after subtracting the background noise.

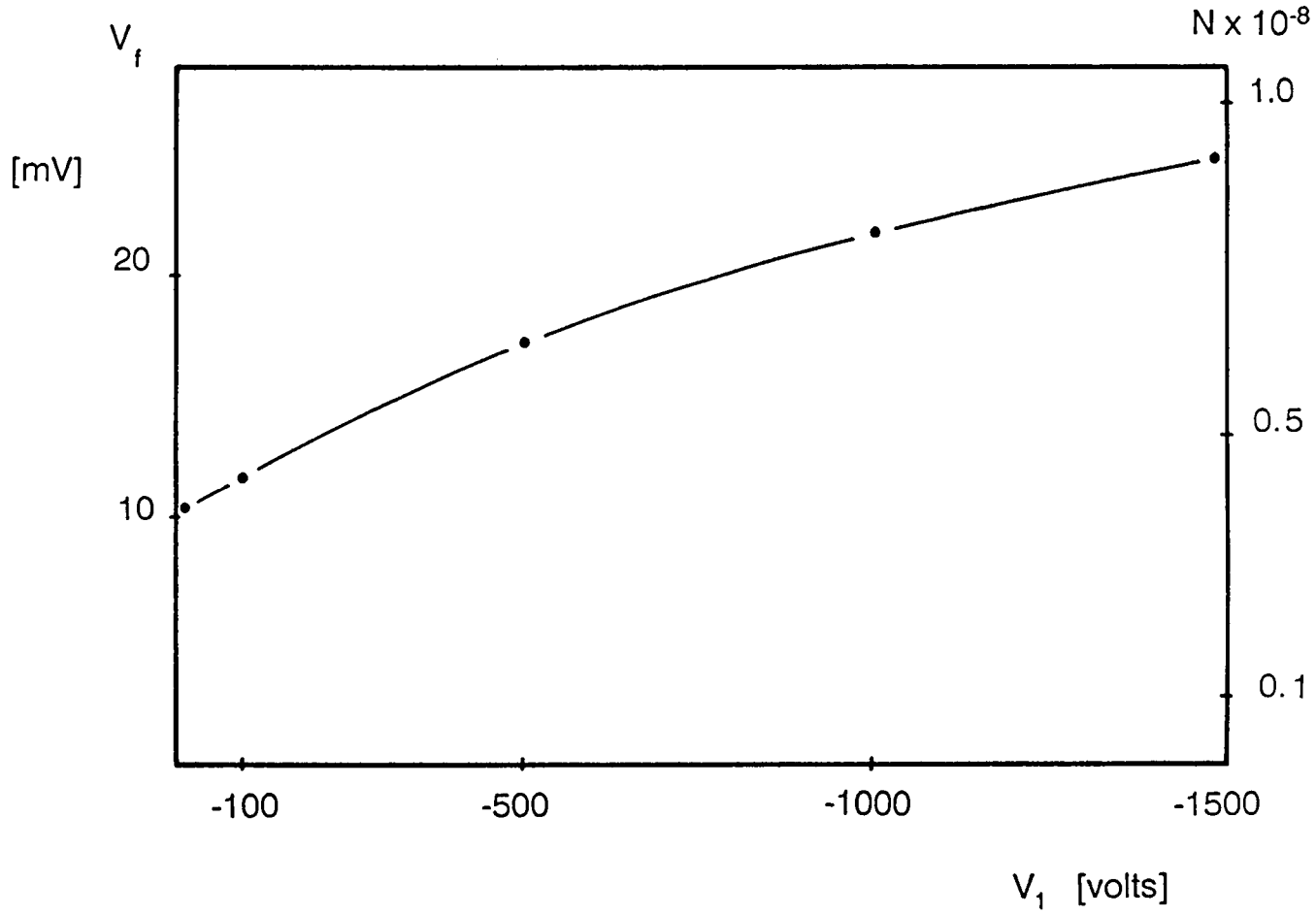

Fig.6: Maximum of the emission signal and the number of electrons emitted from Al as a function of applied negative bias voltage.

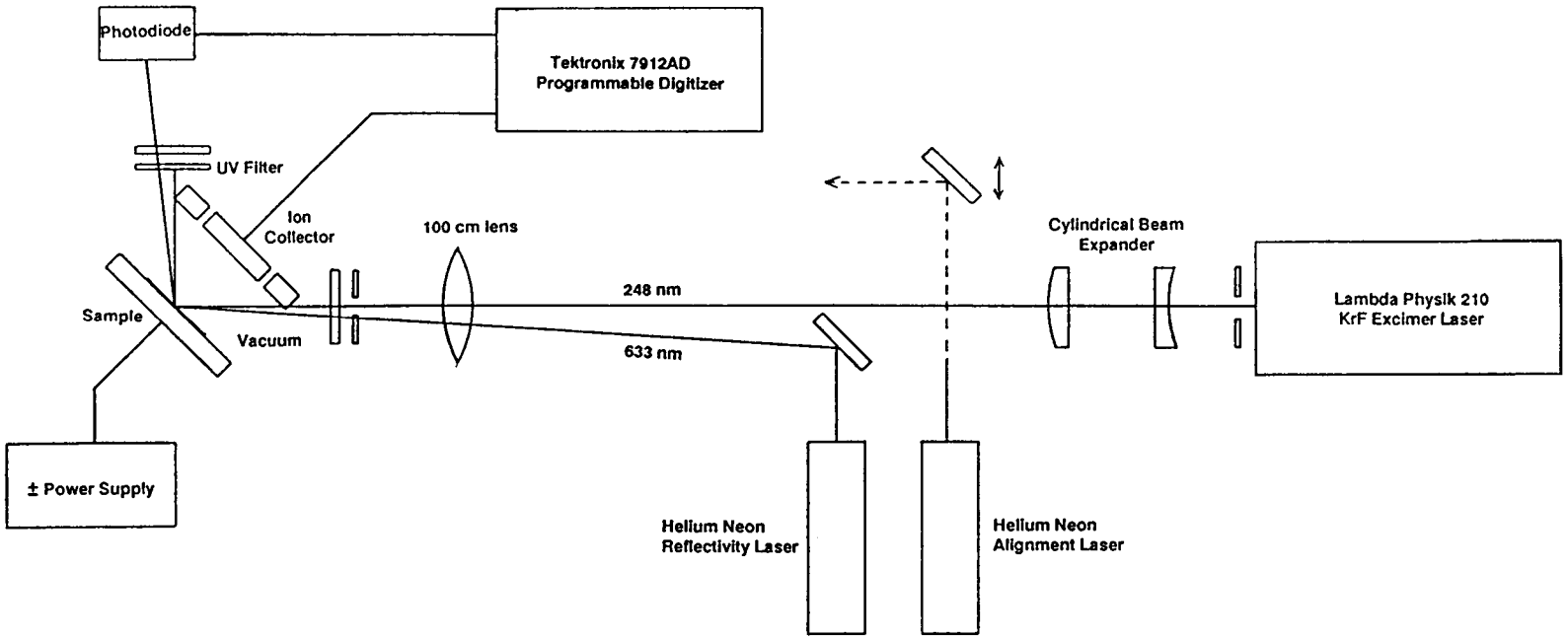

Fig.7: Experimental setup at ORNL.

CHAPTER 4

EXPERIMENTAL RESULTS ON KrF LASER INDUCED CHARGE EMISSION FROM Si AND Ge SURFACES

A. INTRODUCTION

In Chapter 2, we calculated the collection time of electrons and ions. In practice the time of duration t for the signal must satisfy another condition imposed by the collection system, namely:

$$t << RC \qquad (12)$$

In our case R = 50 Ω, C = 240 ppf, thus RC = 12 ns. Although we calculated shorter times of flight for a single free electron, we can see that the total measured signals last longer. One would like RC large compared to the width of the laser pulse to integrate charge. However, the ideal case would be to have RC much less than the width of the laser pulse to record current as a function of time.

We elect to obtain as much information on the current J_e and obtain the charge by integrating over time:

$$q = N e = \int_0^t J_e(t')\, dt' \qquad (13)$$

Output of the emitted charge was regulated by changing the KrF laser energy density. Although we were interested in the charge emission from the melted surfaces, we started the experiment below the melting threshold. We wanted to avoid creating plasma on the surface of the target (which is very undesirable for the RISTRON) and to keep the emission mechanism as simple as possible.

The values of energy density for the KrF laser were estimated by observing the total time of melt, using the change of reflectivity of the HeNe laser beam as an indicator of melting [13]. The changes of reflectivity of Si upon melting are shown in Fig. 8b.

At each energy density level, the emission signals were recorded at target voltages ranging from -2000 to +2000 volts.

B. DATA BELOW THE MELTING THRESHOLD

In order to investigate the emission of negative charge from a solid (unmelted) Ge target we adjusted the KrF excimer laser energy density to approximately E = 250 mJ/cm^2 and used negative bias voltage. The signal obtained seems to be composed of two major signals designated A and B. Part A lasts as long as the KrF laser is illuminating the surface, no matter what bias voltage is applied to the target. Part B of the signal has an amplitude approximately 50% lower; its duration strongly depends on the value of applied voltage and it ends abruptly (Fig.9).

In the case of a Si solid target, the emission was measured for a KrF laser energy density E = 900 mJ/cm^2. Part A of the negative charge signal shows similar behavior as in the case of Ge but part B differs significantly: it lasts longer and seems to decay with an error function (erf) dependence (Fig. 10).

If we changed the bias voltage V_1 from negative to positive in order to measure positive charge emission, the differences between emission signals for Si and Ge became even greater. In the case of Ge they follow almost exactly the KrF excimer laser pulse (Fig. 11), and changing the bias voltage influenced only the amplitude. In the case of Si we obtained a completely different emission

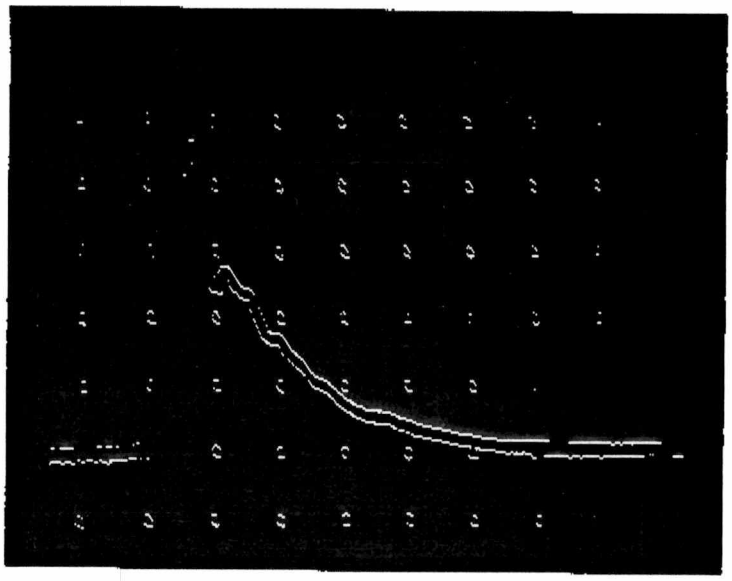

(a)

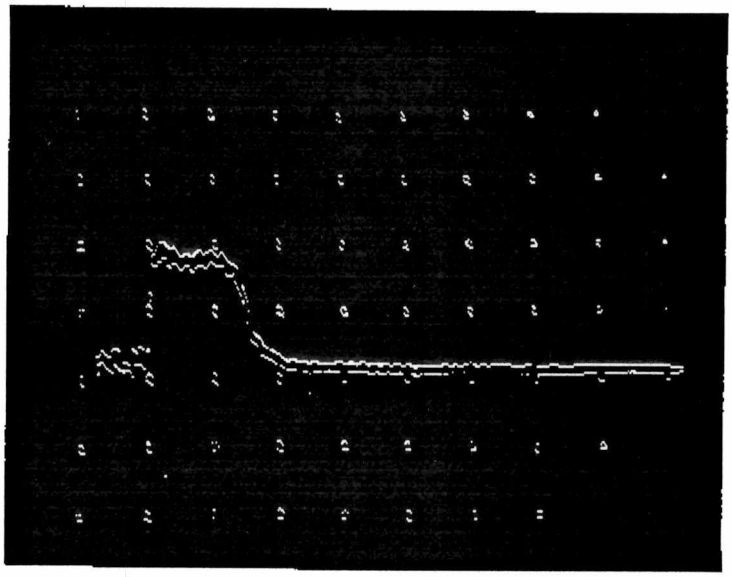

(b)

Fig.8: Original pictures of: a) KrF excimer laser pulse, b) reflectivity of Si when melted by the KrF laser pulse.

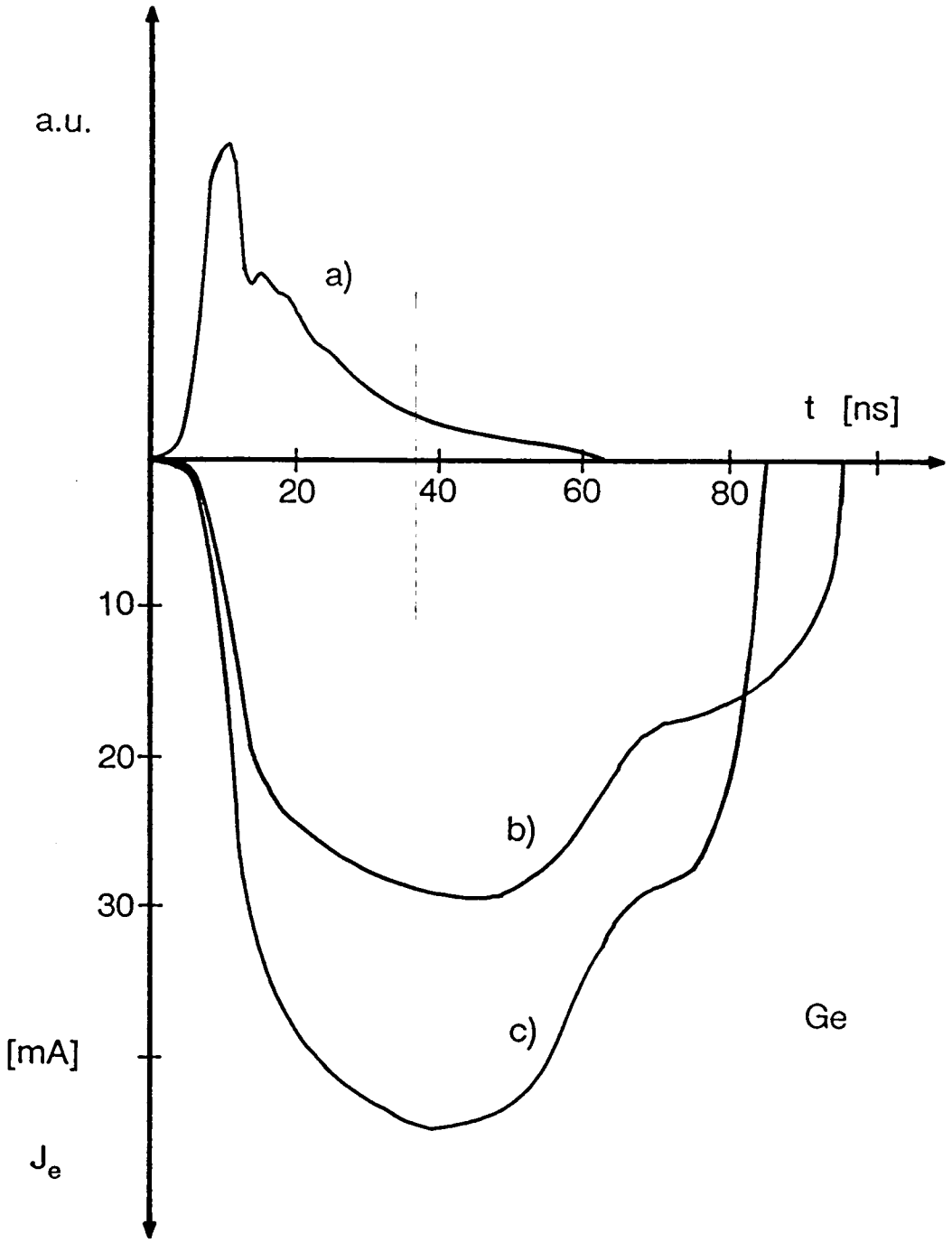

Fig.9: Emission signals for germanium targets below the melting threshold with a negative bias voltage;
a) KrF excimer laser signal,
b) emission signal for E = .25 J/cm^2, V_1 = -1000 V,
c) emission signal for E = .25 J/cm^2, V_1 = -1500 V.

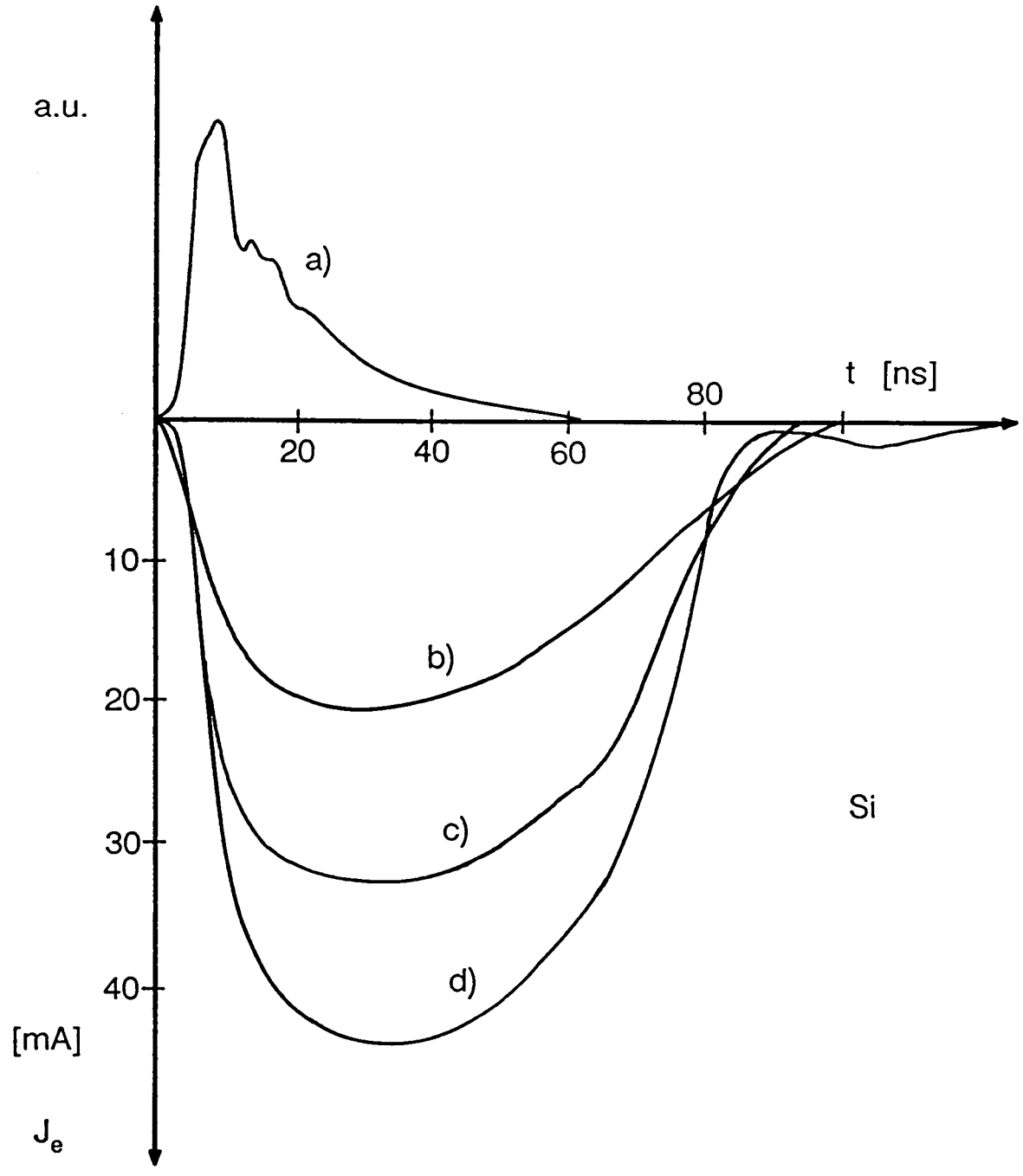

Fig.10: Emission signals for silicon targets below the melting threshold with a negative bias voltage;
a) KrF excimer laser signal,
b) emission signal for E = .9 J/cm^2 , V_1 = -500 V,
c) emission signal for E = .9 J/cm^2 , V_1 = -1000 V,
d) emission signal for E = .9 J/cm^2 , V_1 = -1500 V.

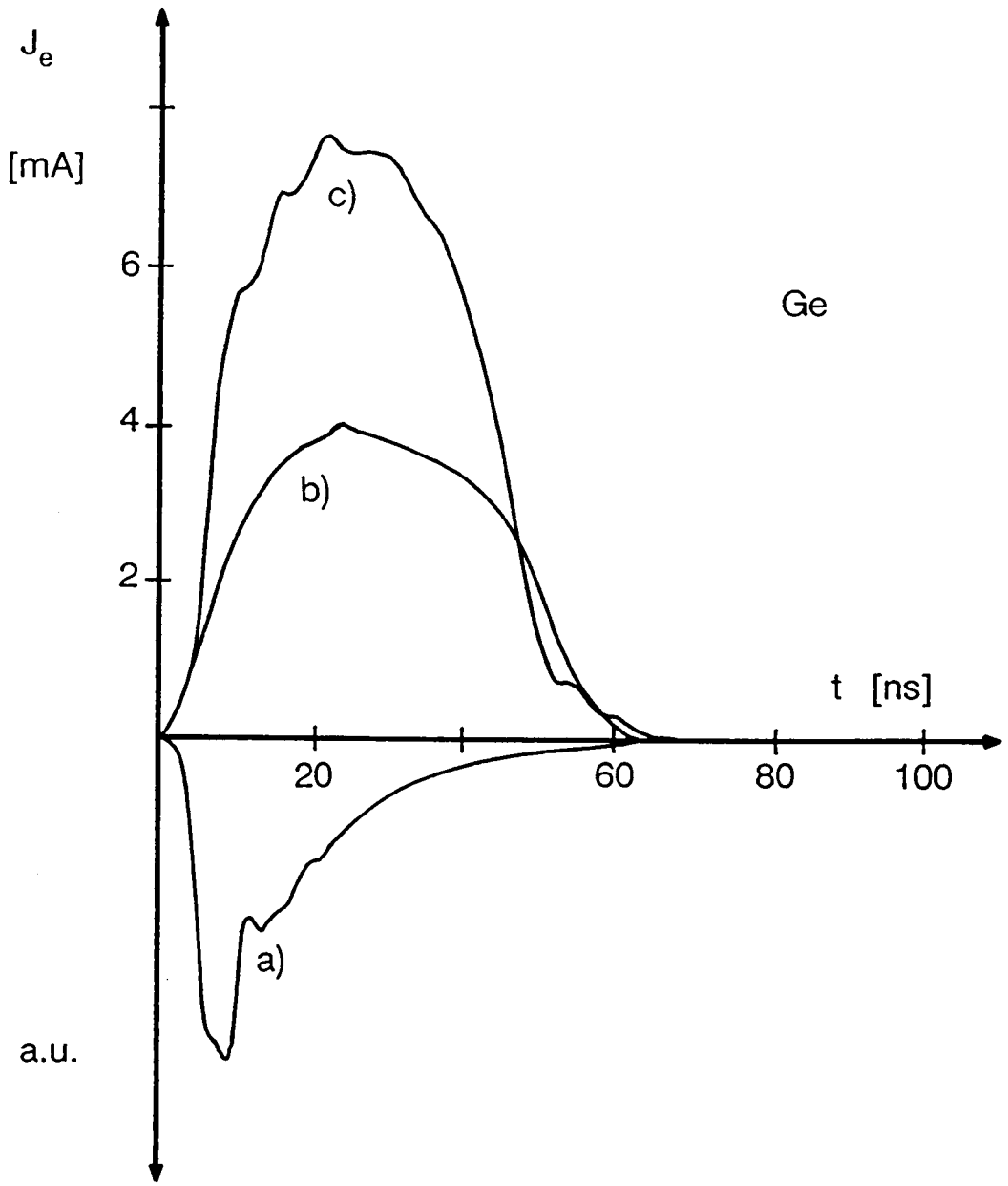

Fig.11: Emission signals for germanium targets below the melting threshold with a positive bias voltage;
a) KrF excimer laser signal,
b) emission signal for E = .25 J/cm^2, V_1 = +500 V,
c) emission signal for E = .25 J/cm^2, V_1 = +1000 V.

signal. It began later than a KrF laser pulse and extended into the microsecond range (Fig. 12). The value of the positive bias voltage strongly affected both the amplitude and the time of the signal emission.

C. DATA ABOVE THE MELTING THRESHOLD

To melt the germanium and silicon wafers' surfaces we increased the KrF laser energy density. To confirm melting and to calculate the laser energy density we measured the reflectivity change with a continuous HeNe laser beam, as noted previously [13].

In the case of a negative bias voltage V_1 (negative charge emission) the emission signals from both materials also had two characteristic parts: part A that seemed to depend strongly on the annealing laser beam and part B that tended to separate from part A with increasing value of energy density. Part B lasted longer than below the melting threshold and decayed in time as an error or exponential functions. For higher energy densities signals from both Si and Ge became almost identical. Emissions from Ge and Si for negative bias voltages are shown in Figs. 13 and 14, respectively.

Emission signals with positively biased targets had the same character as in the corresponding cases below the melting threshold. However, we noticed that for the silicon target, for higher energy densities the emission signals had strong oscillatory character at the beginning. Nanosecond duration signals from positively biased surfaces of Ge were not affected by changing either the KrF laser energy density or the bias voltage, either below and above the melting point.

During the experiments we obtained pictures of more then a hundred emission signals that gave more data then we have shown so far in this thesis. We

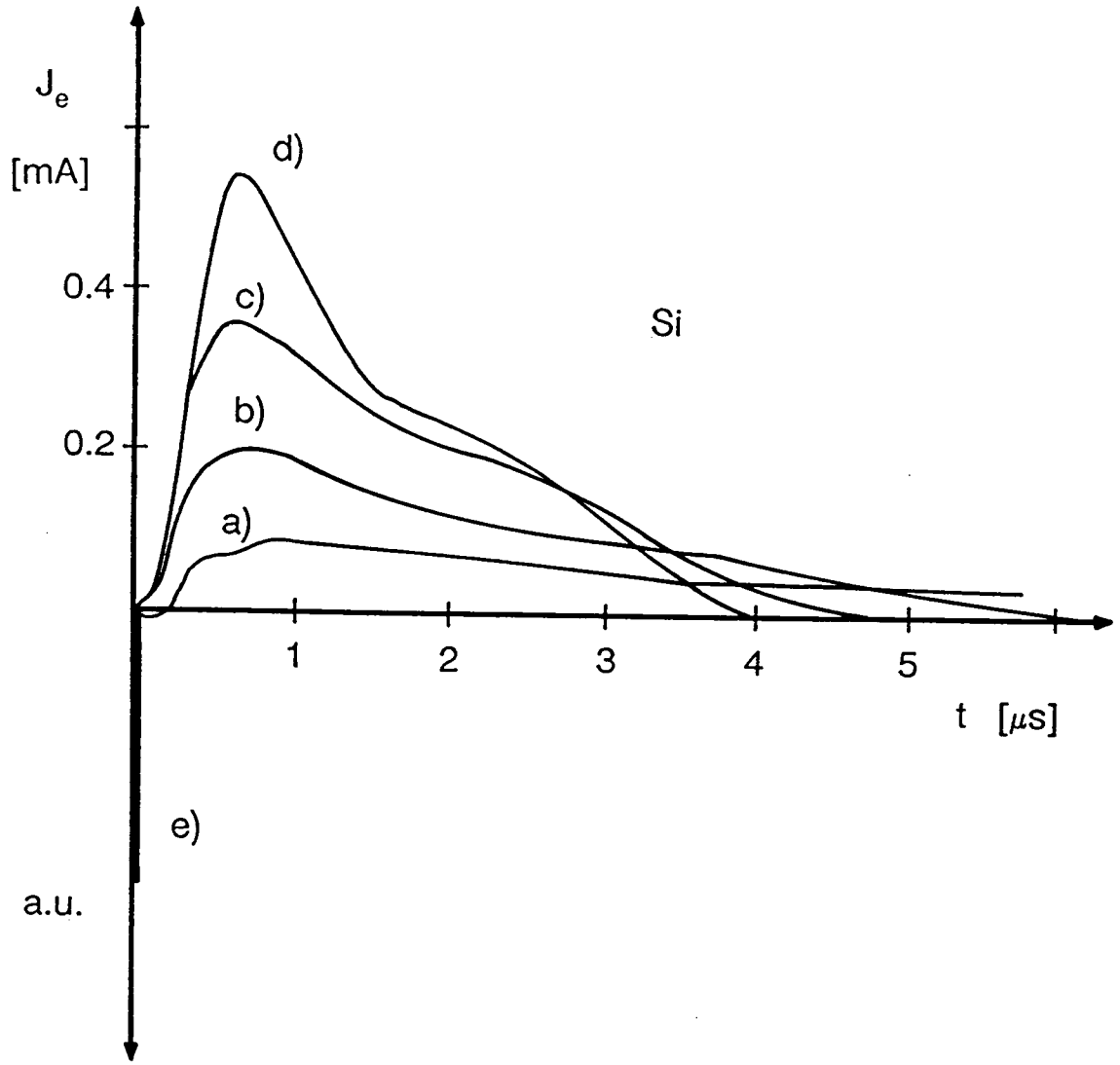

Fig.12: Emission signals for silicon targets below the melting threshold with a positive bias voltage;
a) emission signal for E = .9 J/cm^2, V_1 = +500 V,
b) emission signal for E = .9 J/cm^2, V_1 = +1000 V,
c) emission signal for E = .9 J/cm^2, V_1 = +1500 V,
d) emission signal for E = .9 J/cm^2, V_1 = +2000 V,
e) KrF excimer laser signal.

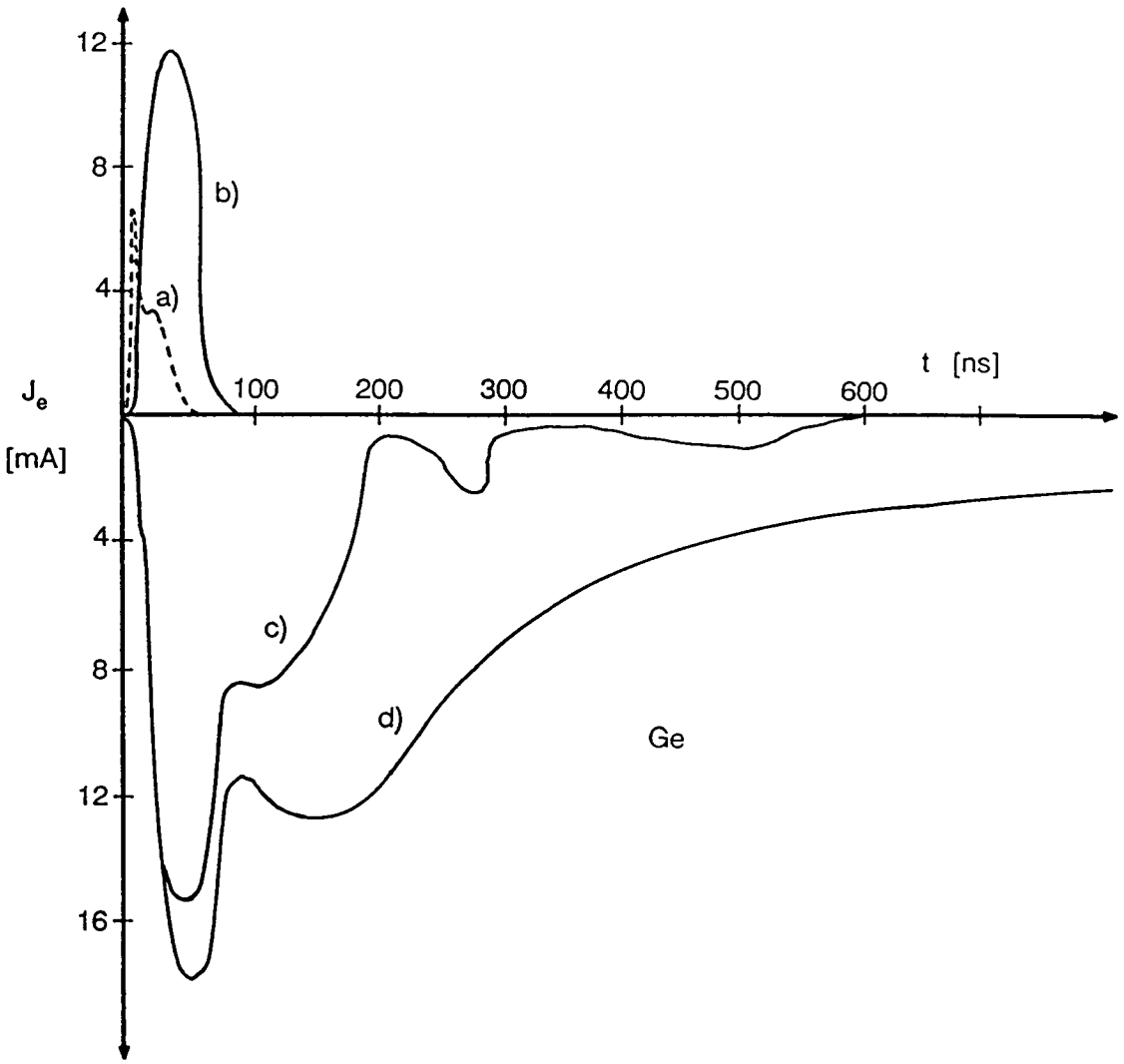

Fig.13: Emission signals for germanium targets above the melting threshold with positive and negative bias voltages;
a) KrF excimer laser signal,
b) emission signal for E = .6 J/cm^2, V_1 = +1000 V,
c) emission signal for E = .35 J/cm^2, V_1 = -500 V,
d) emission signal for E = .6 J/cm^2, V_1 = -500 V.

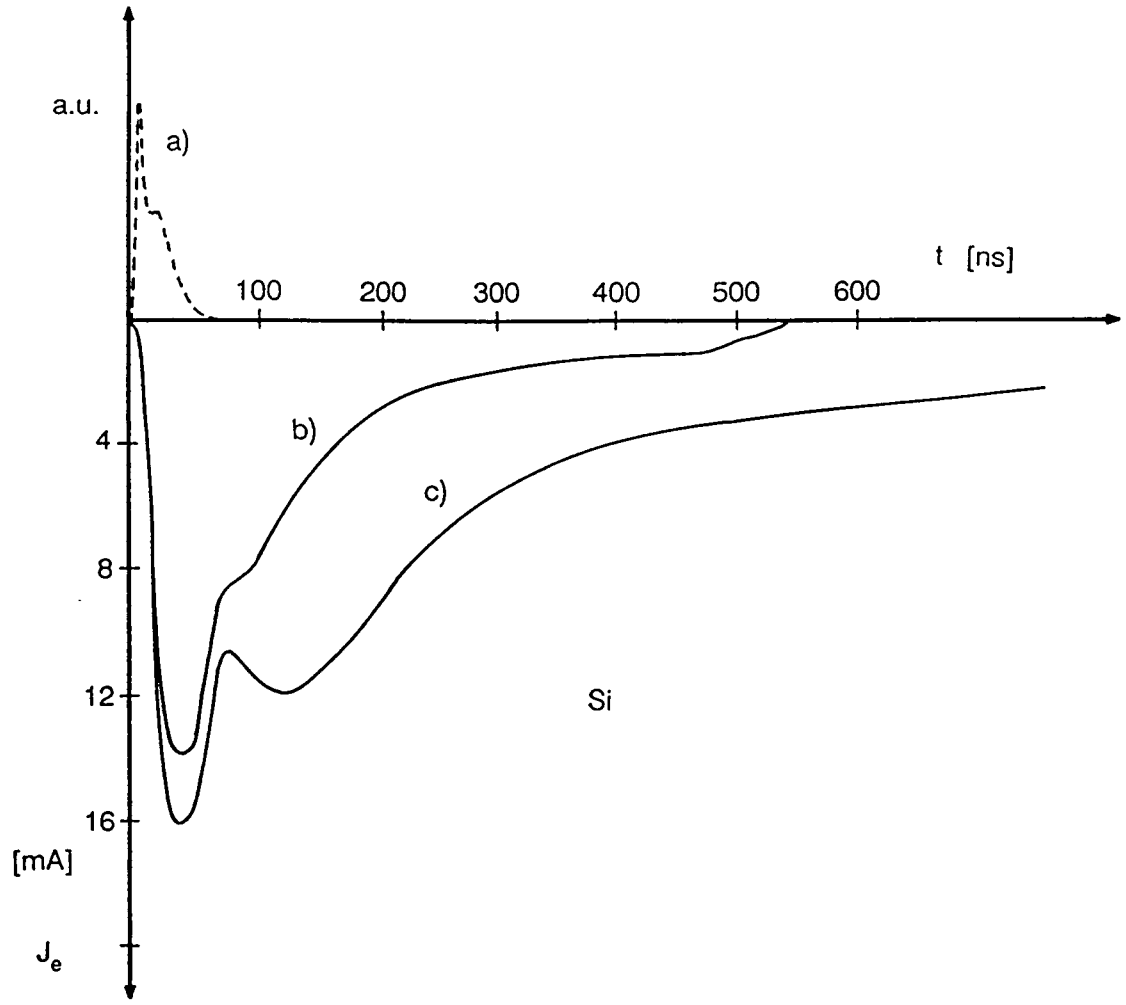

Fig.14: Emission signals for silicon targets above the melting threshold with a negative bias voltage;
a) KrF excimer laser signal,
b) emission signal for E = 1.25 J/cm^2 , V_1 = -500 V,
c) emission signal for E = 1.50 J/cm^2 , V_1 = -500 V.

have summarized these data in a form of graphs in Figs. 15-20 which will be used in our analysis below.

We see that for both Si and Ge, at negative bias voltage the signal maxima occur approximately 30-40 ns after firing the KrF laser and this time is relatively stable. In Figs.15 and 16, we can see that the signal amplitude increases with KrF laser energy density and with the value of bias voltage. The rate of this change is faster for germanium than for silicon.

For both materials the total time of emission decreases as the KrF density decreases and the negative bias voltage increases (compare Fig.17 and Fig.18). The maximum emission of positive charges from Ge and Si increases with increasing positive bias voltage as shown in Figs. 19 and 20.

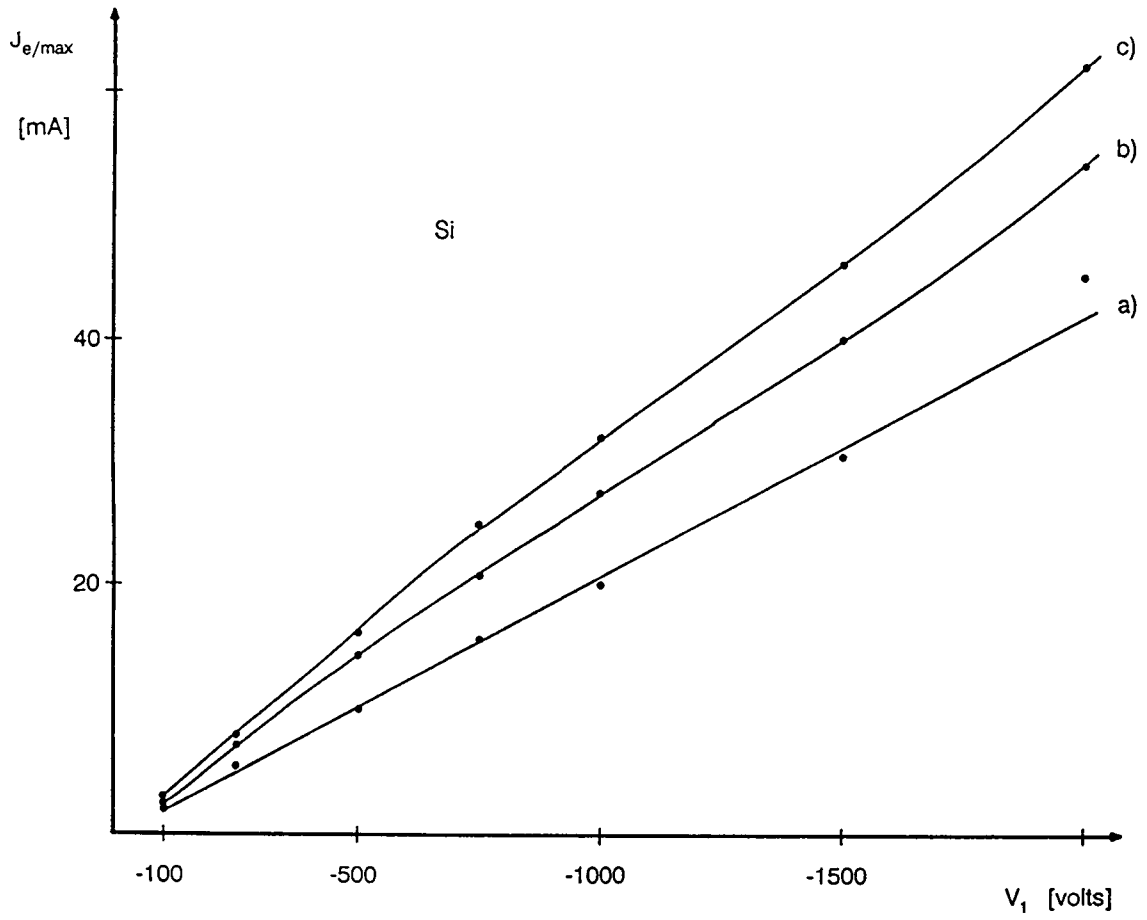

Fig.15: Maxima of the charge emission signals from silicon as a function of applied negative bias voltage;
a) E = .9 J/cm^2,
b) E = 1.25 J/cm^2,
c) E = 1.50 J/cm^2.

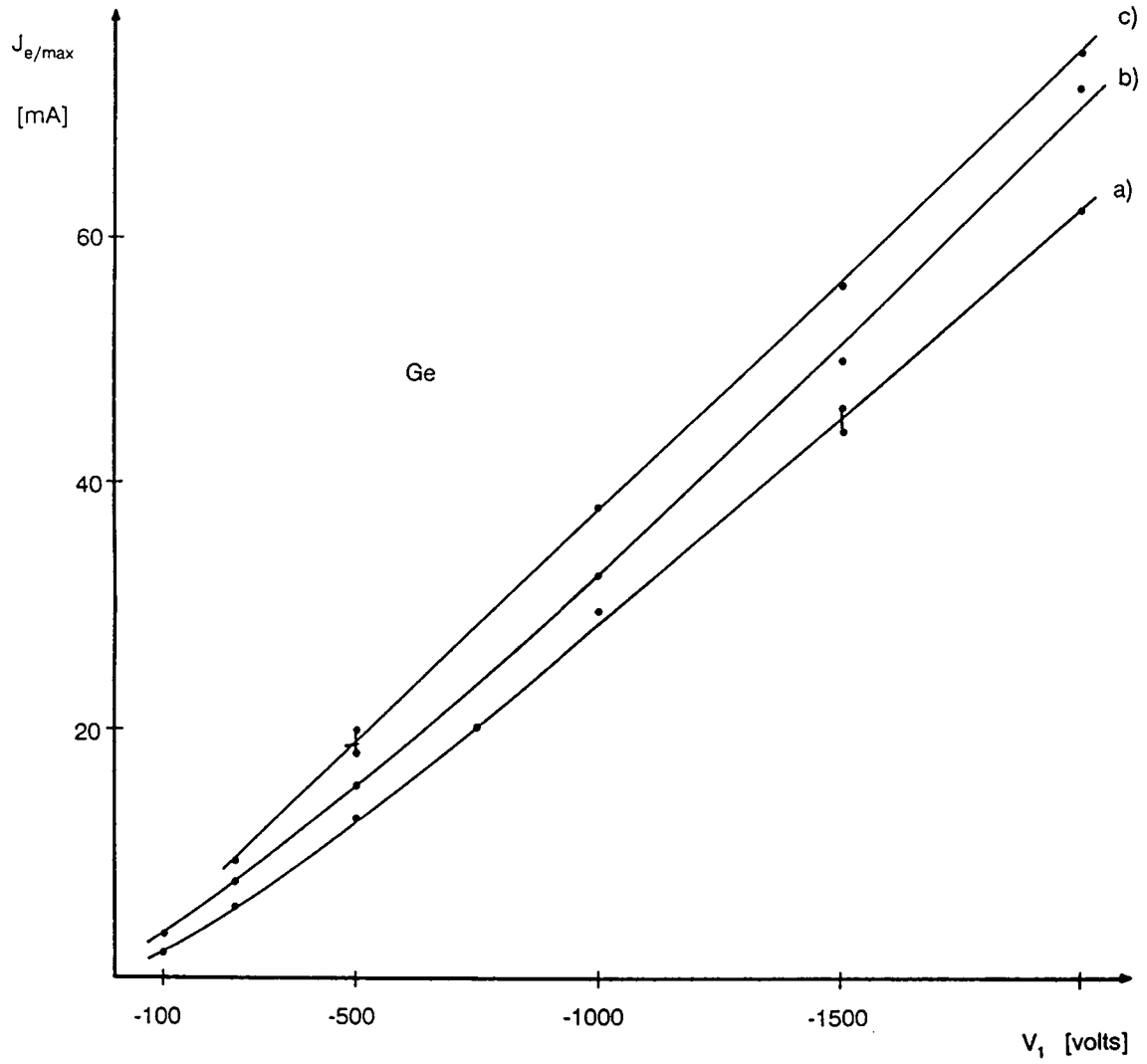

Fig.16: Maxima of the charge emission signals from germanium as a function of applied negative bias voltage;
a) E = .25 J/cm^2,
b) E = .35 J/cm^2,
c) E = .60 J/cm^2.

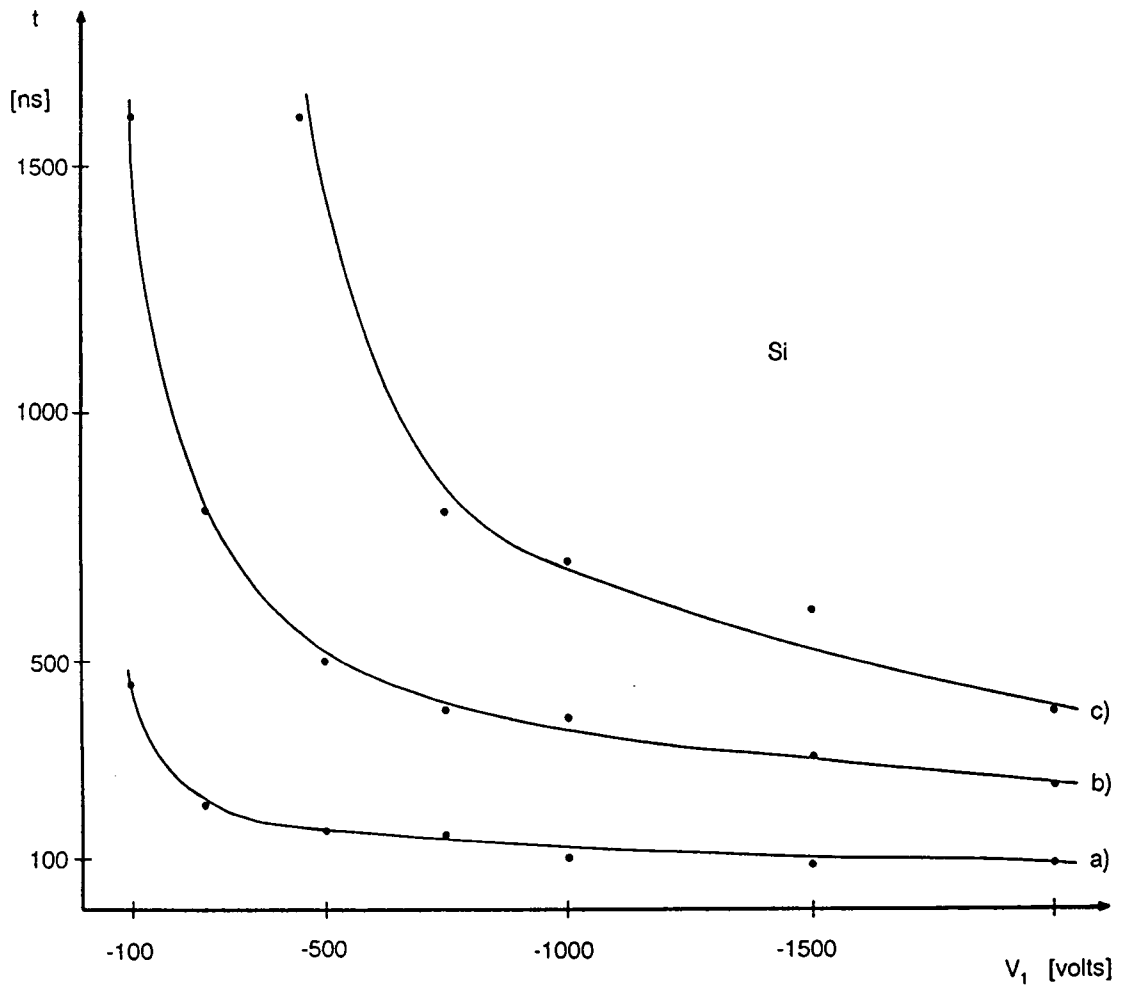

Fig.17: Total time of charge emission for silicon at a negative bias voltage;
a) $E = .9\ J/cm^2$,
b) $E = 1.25\ J/cm^2$,
c) $E = 1.50\ J/cm^2$.

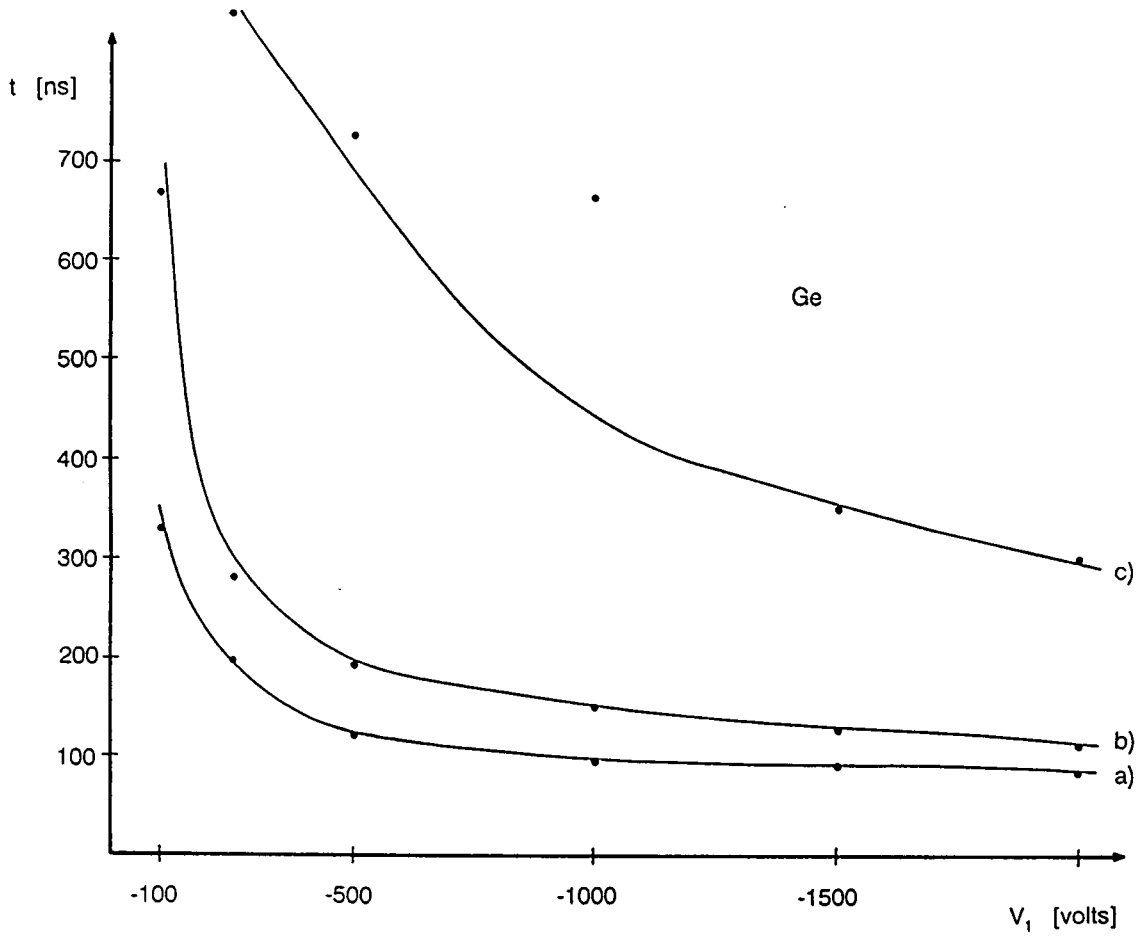

Fig.18: Total time of charge emission for germanium at a negative bias voltage;
a) E = .25 J/cm^2,
b) E = .35 J/cm^2,
c) E = .60 J/cm^2.

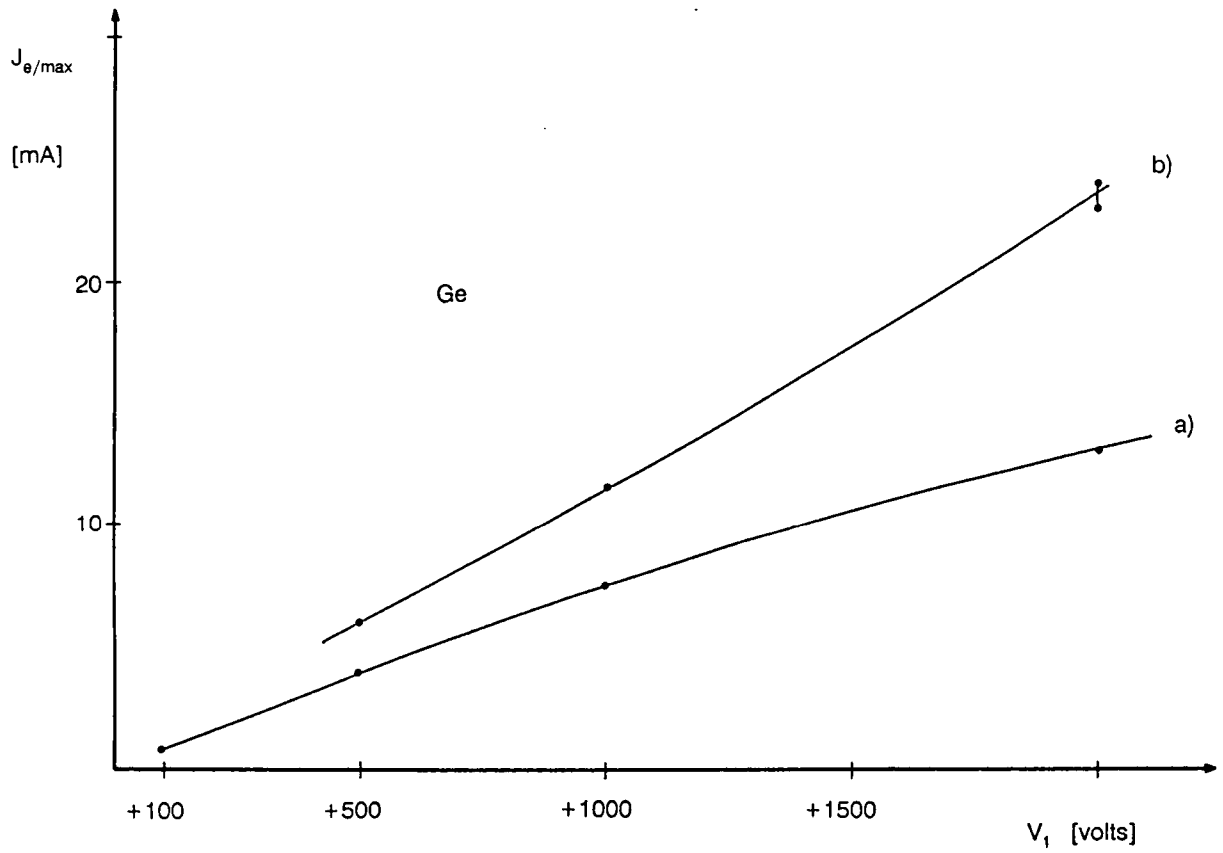

Fig.19: Maxima of the charge emission signals from germanium as a function of applied positive bias voltage;
a) E = .25 J/cm^2,
b) E = .60 J/cm^2.

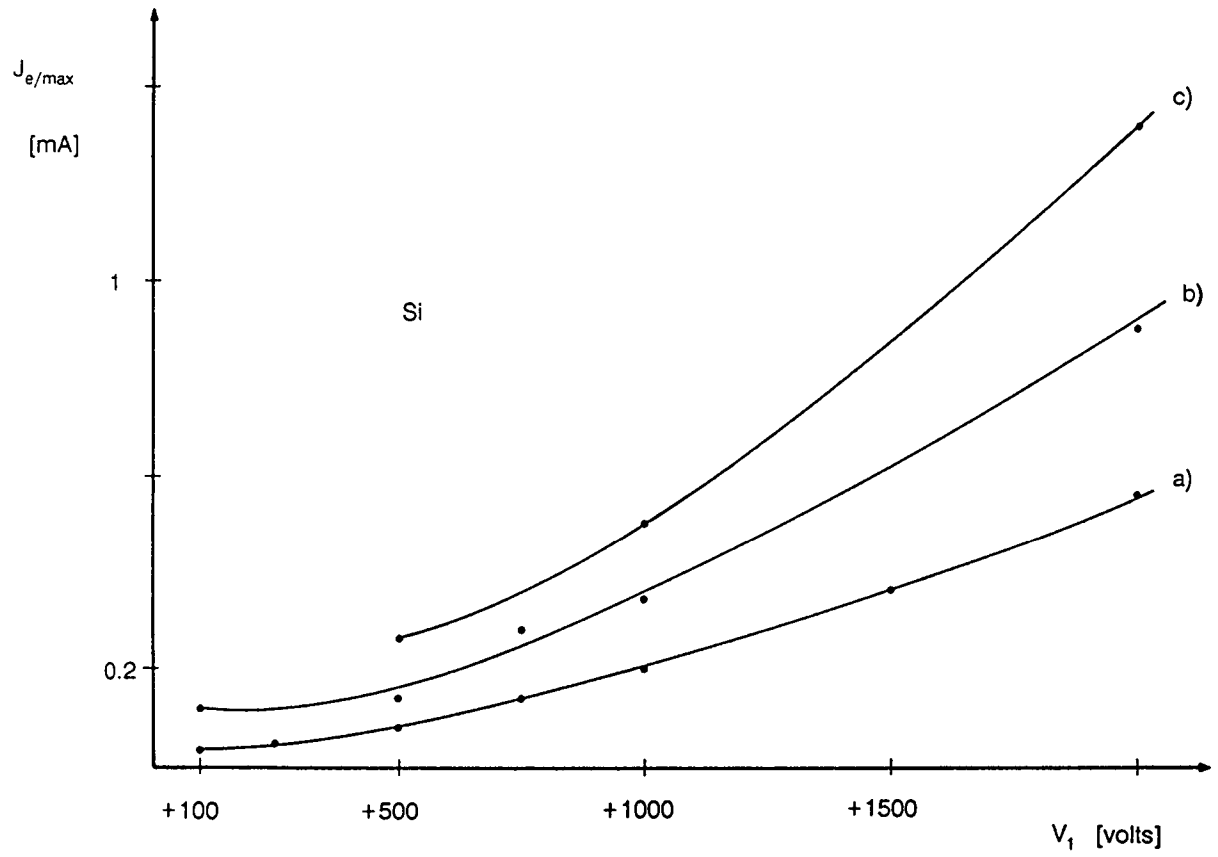

Fig.20: Maxima of the charge emission signals from silicon as a function of applied positive bias voltage;
a) E = .9 J/cm^2,
b) E = 1.25 J/cm^2,
c) E = 1.50 J/cm^2.

CHAPTER 5

DISCUSSION

The RISTRON atom counter utilizes the idea that atoms of interest can be A and Z selected and implanted into the "atom bank." If further isotopic enrichment is necessary, these atoms are removed from the "bank" by pulsed laser melting of the material's surface, again selectively ionized by a RIS laser beam, and after filtering through a mass analyzer, implanted into another "bank" material. This process can be repeated as many times as necessary. Besides sorting, we also can count small populations of atoms during each cycle by monitoring the number of secondary electrons generated by ions striking the target.

One of the main problems that faced the RISTRON project from the beginning was that during laser irradiation of the material a significant amount of charge is emitted. This charge could possibly interfere with transportation of the ions generated by a selective RIS process. The released selected atoms may have velocities on the order of 3 m/s (liquid-solid interface velocity of propagation), implantation depth is about 10 nm, so the whole release process should require only 3 ns. Depending on the RIS laser beam shape and location we should expect Kr atoms to reach the ionization region in about 5 μs. This is the time difference between firing the annealing and the RIS lasers and during this time we have to clear the space of charges generated by the annealing laser.

The results presented in this thesis fully answer the question that has bothered the creators of the RISTRON idea for so long. Experimentally

recorded total times of the charge emission for Si and Ge at different negative bias voltages, plotted in Figs. 17,18, suggest that voltages of a few hundred volts are sufficient to clear the space between the target and the collector of all the charges in less than 1 μs. Thus the results obtained fully satisfy the RISTRON concept requirements and are very optimistic for the future of this device.

Closer analysis of our data shows a surprisingly large and unexpected discrepancy between results for positively biased Si and Ge targets. With positive voltage at the target we expected mainly signals of positive ions to be recorded. For Ge^+ ions the recorded signal lasted approximately as long as the KrF laser was illuminating the sample. Changing the applied positive bias voltage did not effect this time, which seems to contradict our previous calculations, that gave much longer times of flight of Ge^+ between the sample and the collector, on the order of hundreds of nanoseconds. One possible explanation of this effect is that immediately after ejection these ions created heavy, slowly moving clusters that were not recorded at the time scale in use or that they were neutralized by attaching electrons.

Another explanation could be that ejected Ge^+ ions had a very high initial velocity. In order to get more information about how the initial velocity influences the time of charged particle flight in a uniform accelerating electrostatic field we performed additional calculations (Appendix D). The results for different initial velocities and different bias voltages V_1 are shown in Figs. 21-23. These calculations indicate that at negative bias voltages $V_1 > 1000$ volts, the initial velocities do not effect the time of flight very much.

Assuming that there are effects on the surface that give high initial energy to the ejected particles (possible plasma expulsion) we did additional calculations using both analytical and numerical techniques. Sample results of the numerical

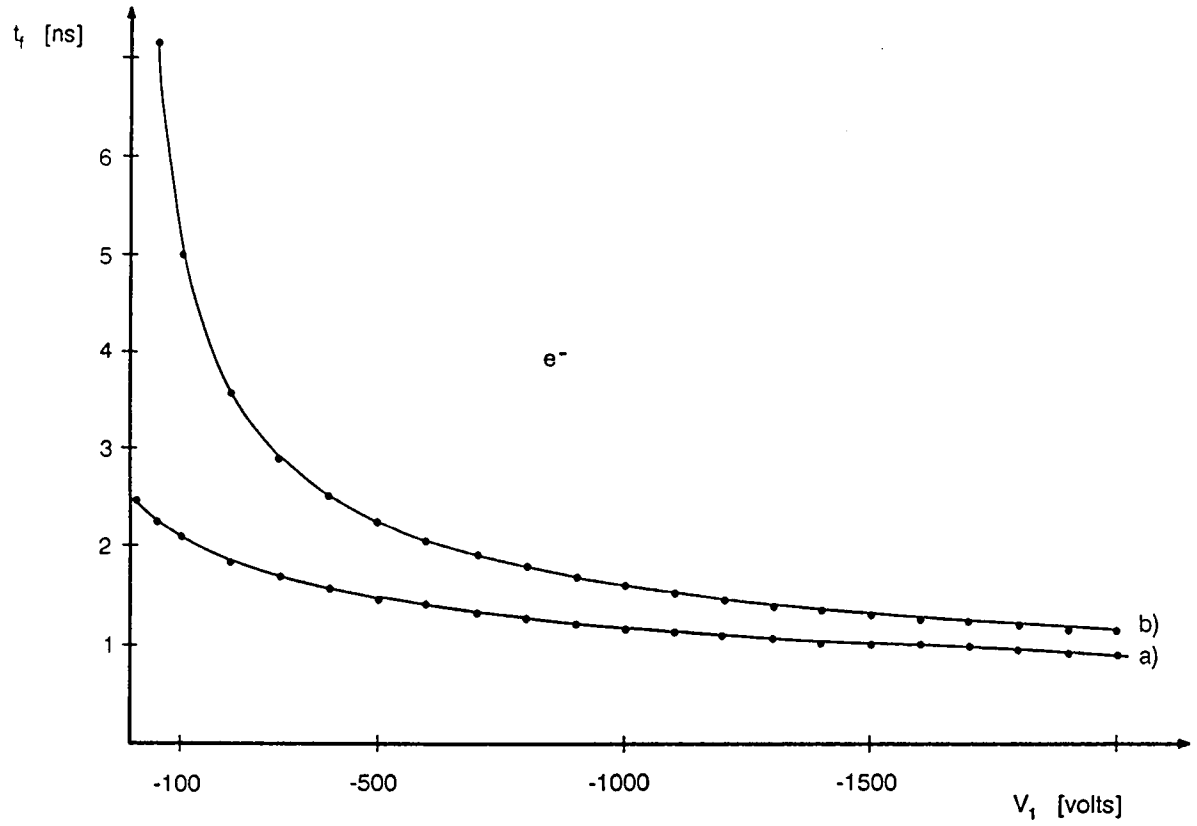

Fig.21: Time of flight of electrons accelerated in a uniform electrostatic field calculated analytically for different initial velocities and bias voltages;
a) $v_o = .6 \cdot 10^7$ m/s,
b) $v_o = 10$ m/s.

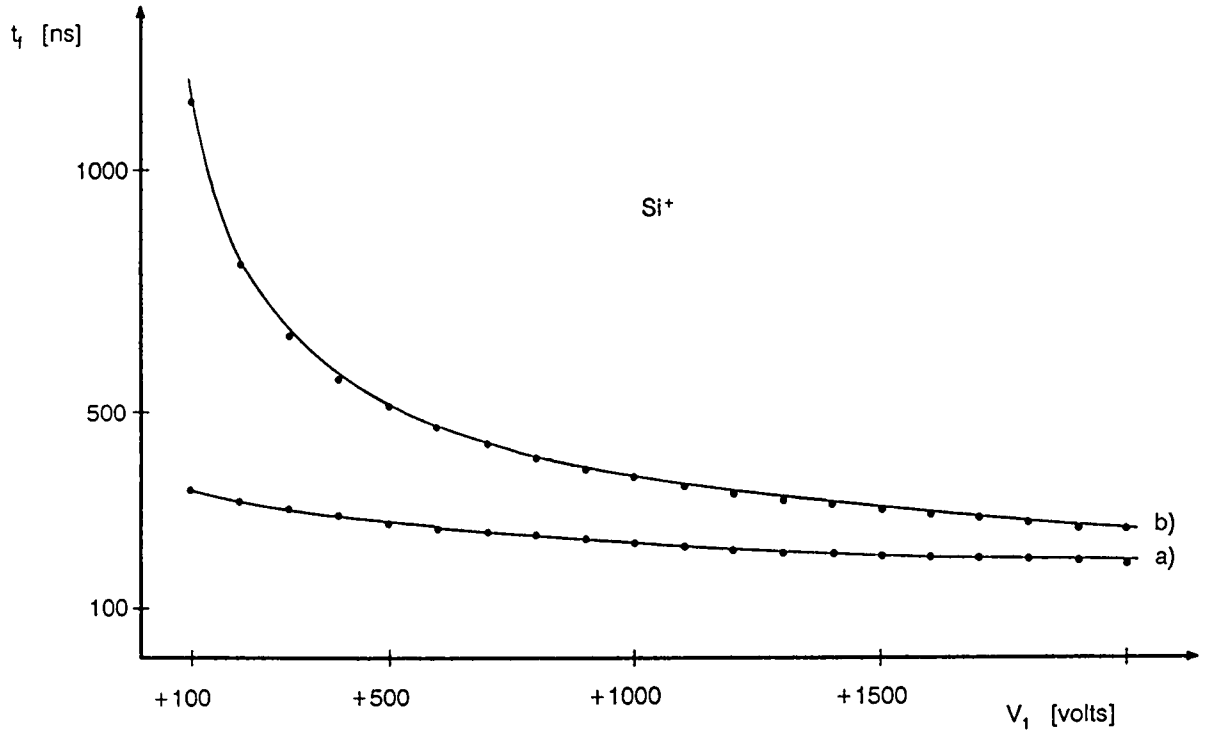

Fig.22: Time of flight of Si^+ ions accelerated in a uniform electrostatic field calculated analytically for different initial velocities and bias voltages;
a) $v_o = 4 \cdot 10^4$ m/s,
b) $v_o = 10$ m/s.

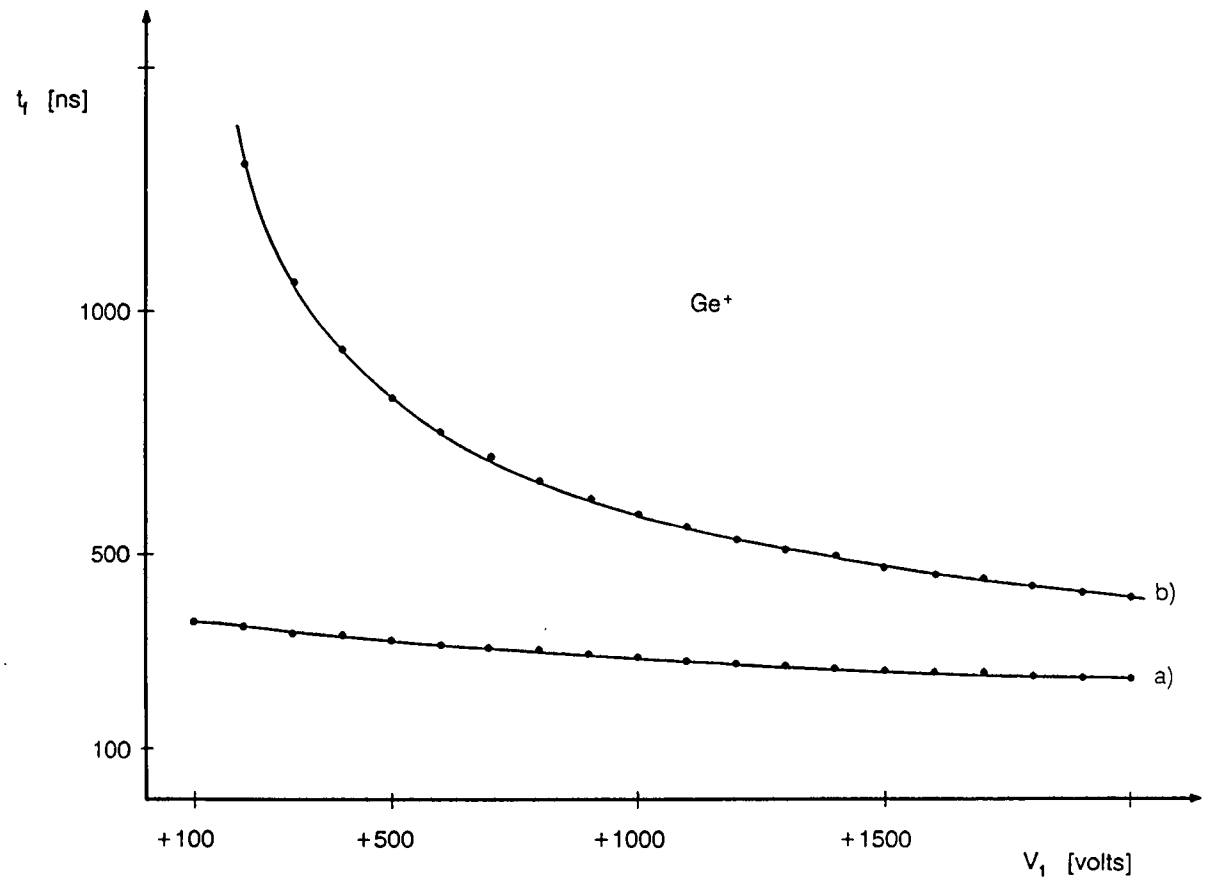

Fig.23: Time of flight of Ge^+ ions accelerated in a uniform electrostatic field calculated analytically for different initial velocities and bias voltages;
a) $v_o = 4 \cdot 10^4$ m/s,
b) $v_o = 10$ m/s.

calculations are presented in Appendix E. This gave us an opportunity to investigate how charges moving against the field forces influence the recorded emission signal. Also, in order to draw more attention to the fact how the electrostatic field deflects the trajectories for realistic voltages and geometries we calculated final radial positions r_f of the particles. These data are presented in Table 5. Their analysis is quite convincing that the motion of charges against the field forces should not influence the emission signal.

Emission signals from the Si target biased by a positive voltage also differ from the results of previous calculations. Nevertheless, the emission time longer than predicted for Si^+ ions is not such a big surprise as the very short emission time observed in the case of positively biased Ge. Laser annealing pulses increase the temperature of the surface and this can result in thermal emission over a longer time as observed for Si. For comparison of differences and analogies between emission signals from Si and Ge surfaces we have presented selected pulses together in Figs. 24-27.

We tried to separate effects that occur during the excimer laser pulse from the total emission, but the phenomenon is too complex to make this separation at the present time. When the surface of the semiconductor material is illuminated by a short pulse of the KrF excimer laser light of high energy density, charge is emitted as a result of many phenomena that happen almost simultaneously. Therefore, it is very difficult to determine to what degree each phenomenon of charge creation contributed to the total charge recorded by the collector. Unfortunately, we do not even know for sure what charges contributed to the recorded current. We expected electrons and singly charged ions but clusters are also possible. If present, we do not know what is their role in the emission signal. They may be fragmented by the excimer laser light or they may attach ions or

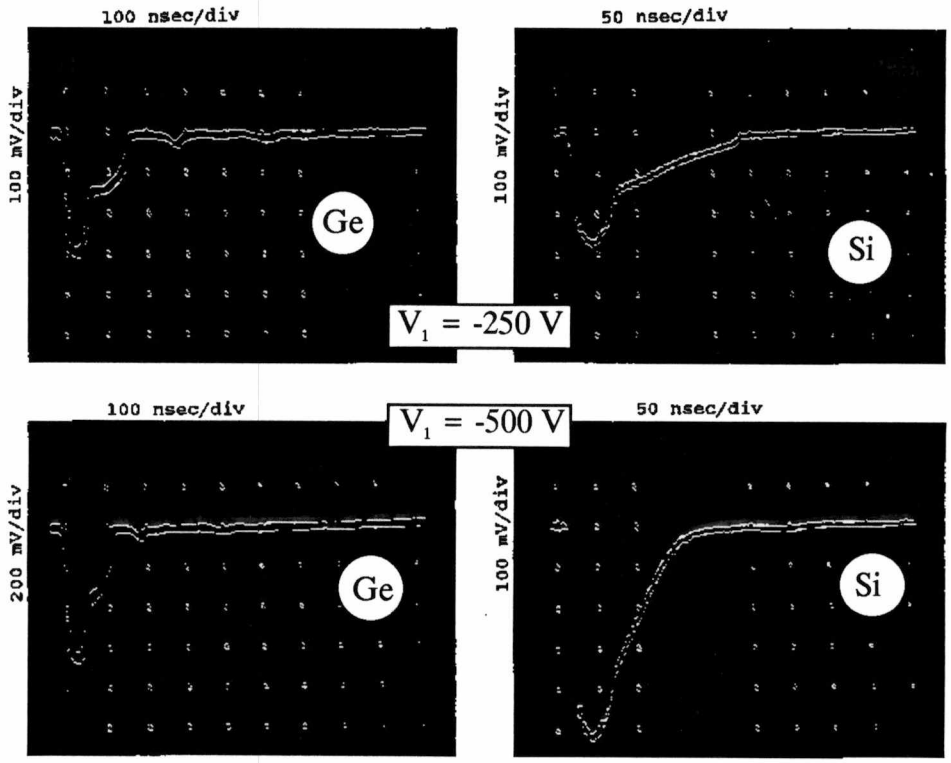

Fig.24: Original emission signals $V_c(t)$ from the solid (unmelted) Ge and Si surfaces biased by a negative voltage V_1, irradiated by KrF laser pulse of energy density E = 250 mJ/cm² for Ge, and E = 900 mJ/cm² for Si.

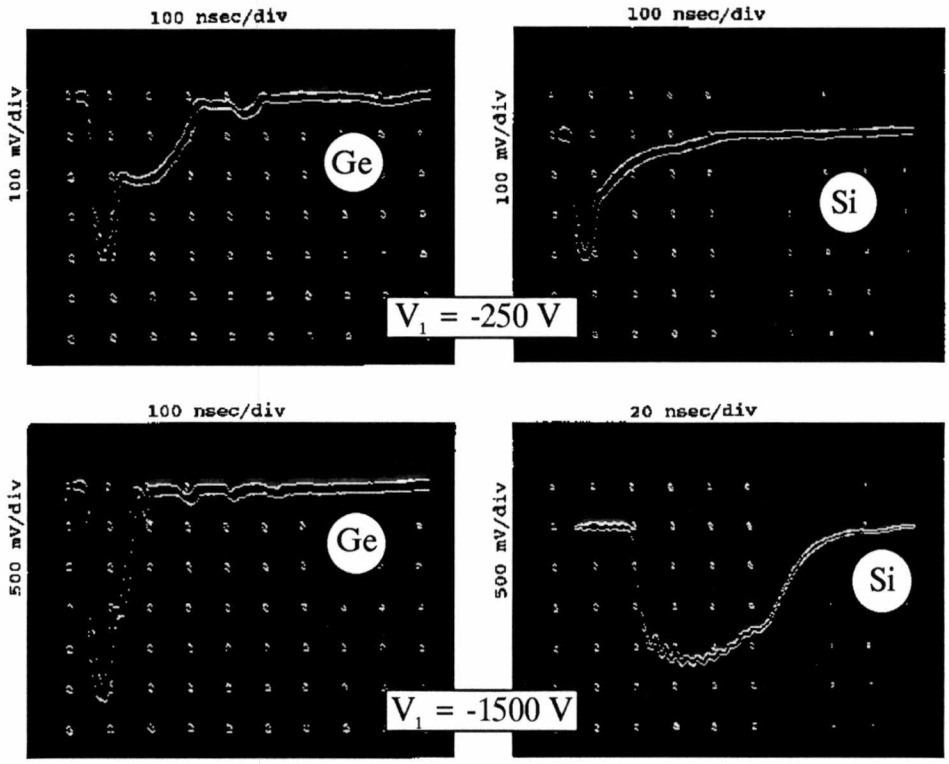

Fig.25: Original emission signals $V_c(t)$ from Ge and Si surfaces biased by a negative voltage V_1, irradiated by a KrF laser pulse of energy density $E = 350\ mJ/cm^2$ for Ge and $E = 1J/cm^2$ for Si.

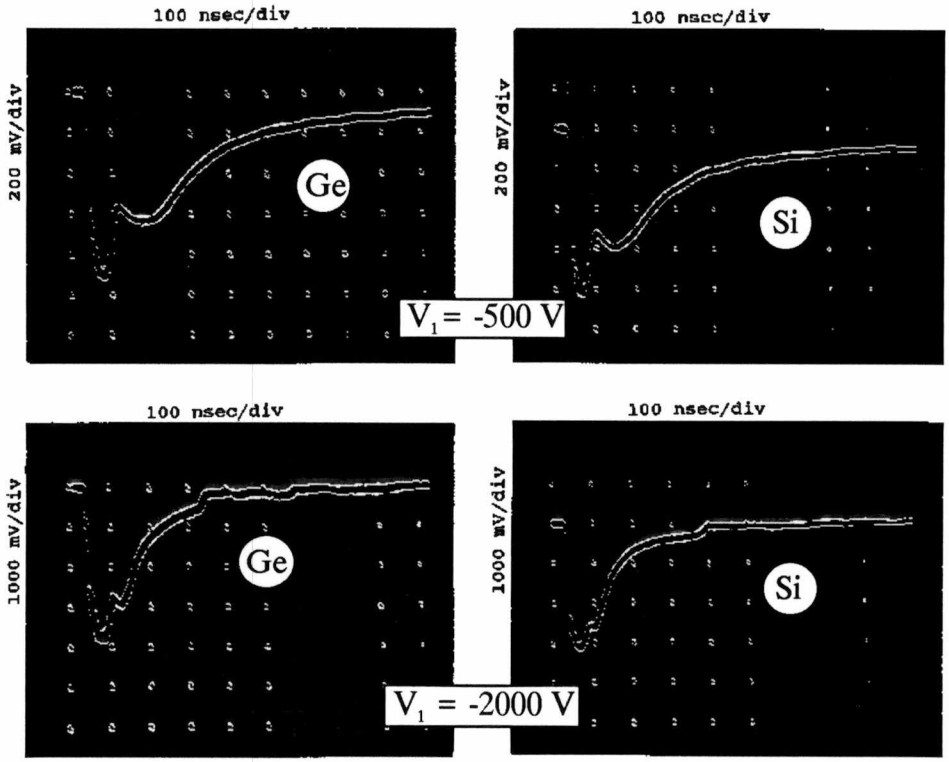

Fig.26: Original emission signals $V_c(t)$ from Ge and Si surfaces biased by a negative voltage V_1 irradiated by a KrF laser pulse of energy density $E = 600\ mJ/cm^2$ for Ge and $E = 1.5J/cm^2$ for Si.

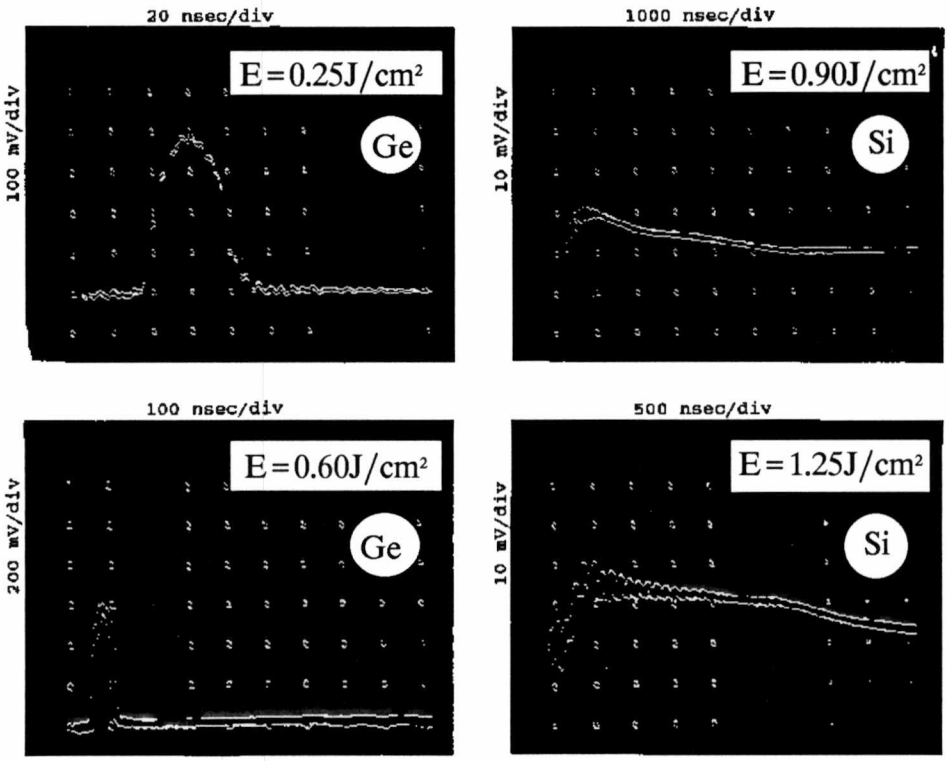

Fig.27: Original emission signals $V_c(t)$ from Ge and Si surfaces biased by positive voltage $V_1 = +1000$ V, irradiated by KrF laser pulses of different energy densities E.

electrons. Also, we did not investigate the behavior of neutrals emitted that may be ionized or highly excited by either of the lasers used.

Yet another one of the possible mechanisms of charge creation in space is energy pooling when highly excited atoms collide giving out positive ions and electrons:

$$Si^* + Si^* \longrightarrow Si_2^+ + e^-$$

Charge emission may also be related to the existence of plasmas, both inside and outside of the material.

As the next step of our analysis we integrated emission currents over time (in practice it was the area under the curve) in order to obtain the total charge emitted. Then, we divided these values by the electron charge = $1.6 \cdot 10^{-19}$ C that resulted in the number of elementary charges in each emission process. This approach may contain some uncertainty because we do not know for sure what are the ways of charge evolution before it reaches the collector. Nevertheless, we have decided to include these results in the thesis in Figs. 28-32. They clearly show that for every applied voltage there are more negative charges than positive ones. For more conclusive analysis we do not have enough data, and the knowledge of the space charge behavior is not sufficient.

Recently, Giammanco has presented a model of electrons and ions' space-time evolution following laser annealing using the fluid approach with the aim of describing the interactions between charged species [39]. In a very interesting experiment [40] on three-photon ionization of Na with a pulsed dye laser he

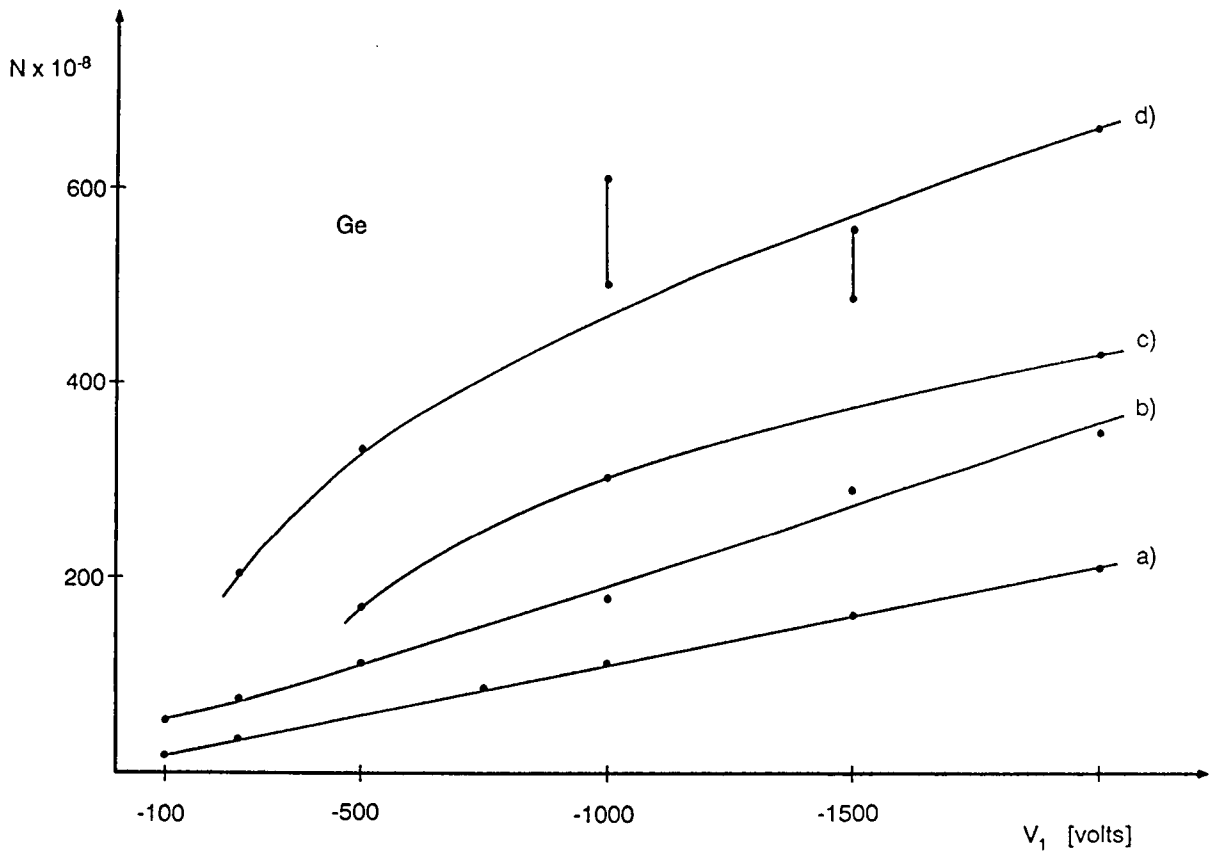

Fig.28: Number of electrons emitted from Ge at negative bias voltages;
a) E = .25 J/cm^2,
b) E = .35 J/cm^2,
c) E = .50 J/cm^2,
d) E = .60 J/cm^2.

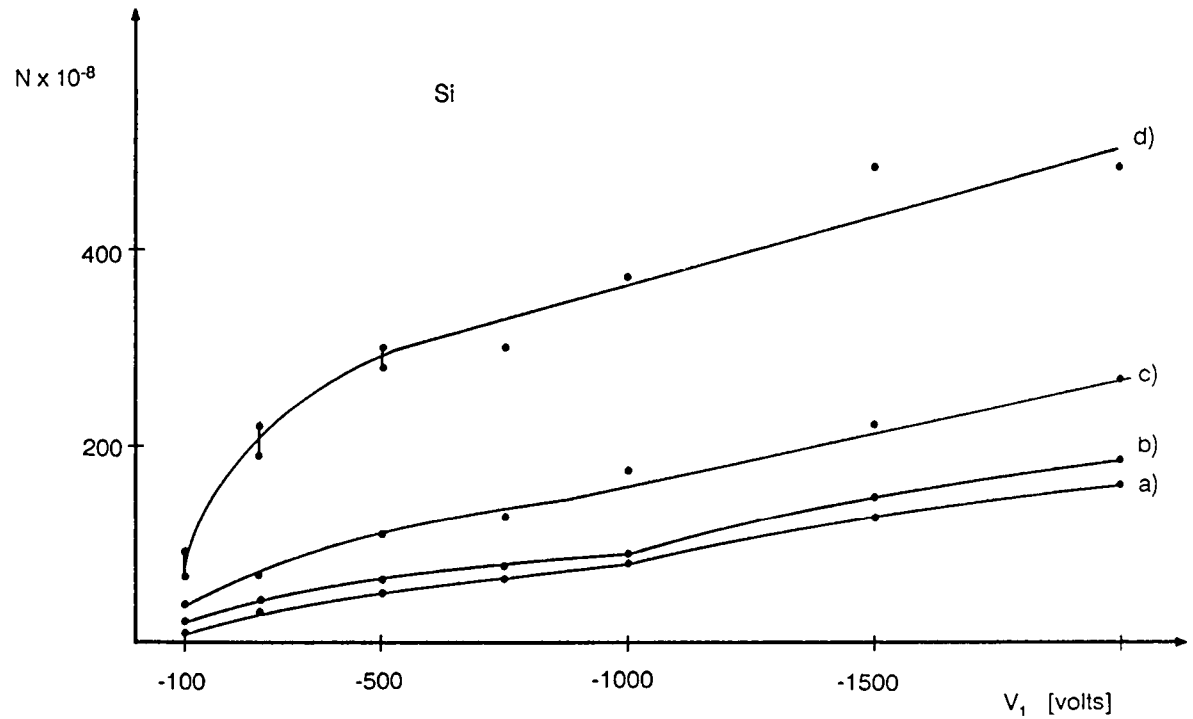

Fig.29: Number of electrons emitted from Si at negative bias voltages;
a) $E = 0.90\ J/cm^2$,
b) $E = 1.0\ J/cm^2$,
c) $E = 1.25\ J/cm^2$,
d) $E = 1.5\ J/cm^2$.

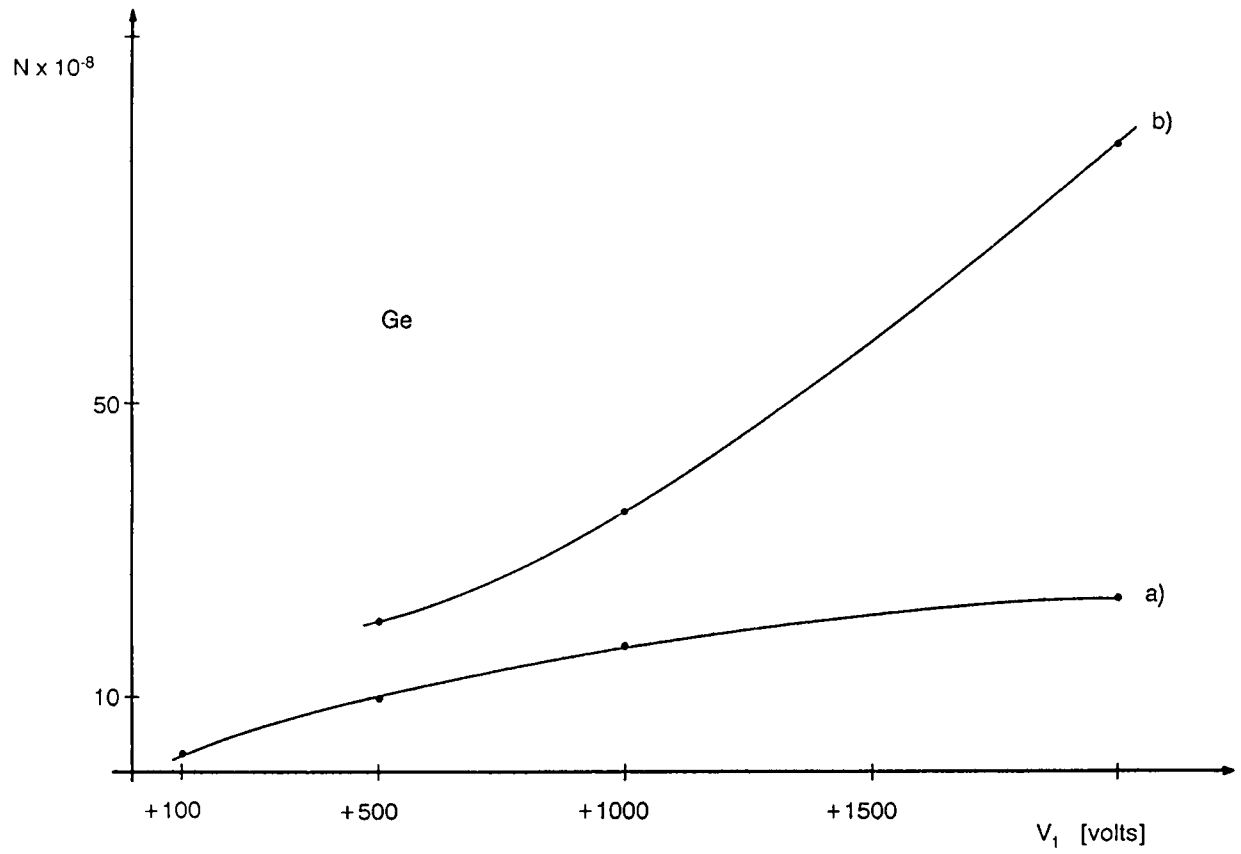

Fig.30: Number of ions emitted from Ge at positive bias voltages;
a) E = .25 J/cm^2,
b) E = .60 J/cm^2.

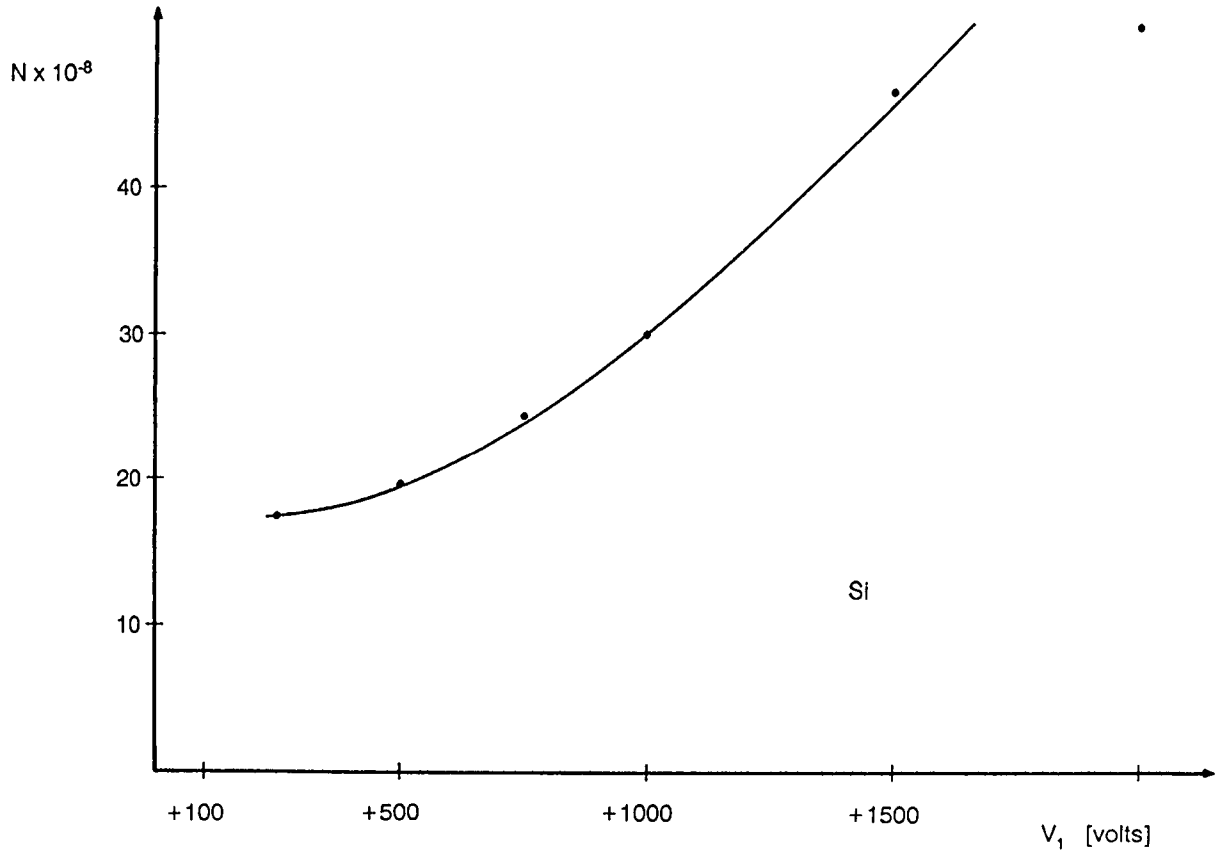

Fig.31: Number of ions emitted from Si at positive bias voltages;
E = .90 J/cm^2.

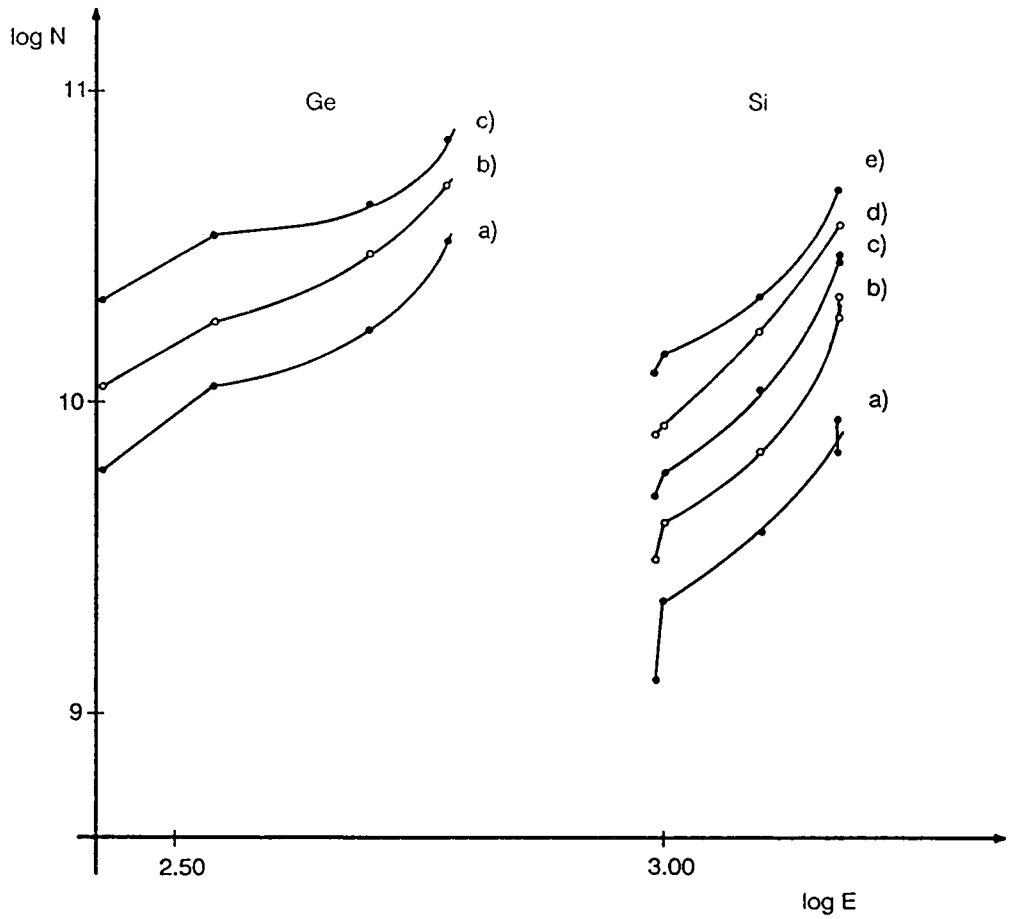

Fig.32: Number of electrons emitted from Ge and Si versus KrF laser energy density on a log-log scale;
Ge: a) V_1 = -500 V, b) V_1 = -1000 V, c) V_1 = -2000 V,
Si: a) V_1 = -100 V, b) V_1 = -250 V, c) V_1 = -500 V,
d) V_1 = -1000 V, e) V_1 = -1500 V.

obtained signals of electron current in an externally applied electric field. Their shape, although recorded by a different technique, resembles some of the emission pulses we have obtained and presented in this thesis (Fig.26).

CHAPTER 6

CONCLUSIONS

As a part of the RISTRON project, our experiment started with the purpose of investigating the time behavior of the space charge produced during excimer laser irradiation of Si and Ge. We wished to confirm that it could be removed in a time shorter than 5 μs. As the data presented here show, this has been achieved very satisfactorily. But the emission signals show unpredicted functional dependences on time. These can be attributed either to some unknown properties of Si and Ge under our experimental conditions and/or to more complicated charge evolution in the space between the target and the collector.

The importance of Ge and Si in technology requires detailed knowledge of the behavior of these materials and the questions that have been raised by this experiment should be answered.

Question 1: What are the species emitted from the surface and what is their behavior before they reach the collector?

Question 2: What different charge emission phenomena occur, when do they occur, and what is their share in the overall effect?

Question 3: Why do we get such different emission signals for Ge and Si, and what properties of these materials are responsible for these differences?

The answers to these questions may give new insight into the Si and Ge.

It would be very interesting to do similar experiments with other

technologically important materials: GaAs, graphite, Au, ... The experimental setup could be improved by adding a mass spectrometer to investigate the species emitted from the surface. In addition, the geometry and time resolution of the system would need to be improved.

REFERENCES

REFERENCES

[1] G.S. Hurst et al., Rep. Prog. Phys., 58 (1985), 1333

[2] G.S. Hurst, M.G. Payne, Resonance Ionization Spectroscopy 1984, eds. G.S. Hurst, M.G. Payne [Bristol: Institute of Physics (Conference Series No. 71)], 309

[3] G.S. Hurst, S.L. Allman, Noble Gas Atom Counter Utilizing Laser Annealing and Resonance Ionization Spectroscopy (Patent disclosure CNID - 4403), 1983

[4] G.S. Hurst, M.G. Payne, Principles and Applications of Resonance Ionization Spectroscopy, Bristol, 1988, ed. Adam Hilger

[5] G.S. Hurst et al., Resonance Ionization Spectroscopy 1988, eds. T.B. Lucatorto, J.E. Parks [Bristol and Philadelphia: Institute of Physics (Conference Series No. 94)], 229

[6] G.S. Hurst et al., Final Report on Phase I, NSF SBIR Grant No. 151-8760496

[7] D.R. Corson, R.R. Wilson, Rev. Sci. Inst. 19 (1948), 207

[8] J.F. Ready, J. Appl. Phys. 36 (1965), 462

[9] J.F. Ready, Effects of High-Power Laser Radiation, Academic Press, New York, 1971

[10] J.H. Bechtel, J. Appl. Phys. 46 (1975), 1585

[11] N. Bloembergen, Laser-Solid Interactions and Laser Processing, 1978, eds. S.D. Ferris et al. [Boston: Mat. Res. Soc.], 1

[12] N. Bloembergen et al., Mat. Res. Soc. Symp. Proc., 51 (1985), 3

[13] G.E. Jellison, Jr. et al., Proceedings of SPIE, 710 (1986),24

[14] M.I. Gallant, H.M. Van Driel, Phys. Rev. B26 (1982), 2133

[15] J.S. Preston, H.M. Van Driel, Phys. Rev. B30 (1984), 1950

[16] N. Bloembergen et al., Laser and Electron-Beam Interactions with Solids, eds. B.R. Appleton, G.K. Celler, 1982, 3

[17] L.A. Lompre et al., Appl. Phys. Lett., 44 (1983), 3

[18] A. Aydinh et al., Phys. Rev. Lett., 46 (1981), 1640

[19] J.F. Ready, Phys. Rev., 137 (1965), A620

[20] B. Stritzker et al., Phys. Rev. Lett., 47 (1981), 356

[21] A. Pospieszczyk et al., J. Appl. Phys., 54 (1983), 3176

[22] J.S. Preston, H.M. Van Driel, Phys. Rev., B30 (1984), 1950

[23] D.H. Lowndes et al., Phys. Rev., B26 (1982), 6747

[24] J.A. Van Vechten et al., Phys. Lett., A74 (1979), 417

[25] J.A. Van Vechten, Laser and Electron-Beam Interaction with Solids, eds. B.R. Appleton, G.K. Celler, 1982, 49

[26] C. Peugnet, J. Appl. Phys., 48 (1977), 3206

[27] T.T. Tsong, J. Vac. Sci. Technol., B3 (1985), 1425

[28] T.T. Tsong, Phys. Rev., B30 (1984), 4946

[29] D. Lubben et al., J. Vac. Sci. Technol., B3 (1985), 968

[30] M. Hanabusa et al., Appl. Phys. Lett., 38 (1981), 385

[31] G.B. Shinn et al., J. Vac. Sci. Technol., B4 (1986), 1273

[32] J.H. Bechtel et al., Phys. Rev., B15 (1977), 4557

[33] J.M. Liu et al., Appl. Phys. Lett., 39 (1981), 755

[34] J.M. Liu, Laser and Electron-Beam Interaction with Solids, eds. B.R. Appleton, G.K.Celler, 1982, 29

[35] A.M. Malvezzi et al., Appl. Phys., A36 (1985), 143

[36] A.M. Malvezzi et al., Mat. Res. Soc. Symp. Proc., 23 (1984), 135

[37] A.M. Malvezzi et al., Mat. Res. Soc. Symp. Proc., 35 (1985), 75

[38] A.M. Malvezzi et al., "Beam-solid Interactions and Phase Transformations," eds. H. Kurz, G.L. Olson and J.M.Poate, Mat. Res. Soc. Symp. Proc., 51 (1986) 201.

[39] F. Giammanco, Phys. Rev., A 36 (1987), 5658

[40] F. Giammanco, Phys. Rev., accepted for publication

APPENDICES

APPENDIX A

Electrical Potential W and Field F Distribution in a Conducting Cylindrical Box

Potential W obtained by an analytical solution of Laplace's eq.:

$$\nabla^2 W = 0$$

$$W(z,r) = \sum_{i=0}^{\infty} \{ A_i \exp(a_i z) + B_i \exp(-a_i z) \} \cdot J_o(r a_i)$$

where:

$2\,a_i$ = i-th root of Bessel function of the zero-th order; A_i, B_i = coefficients of the i-th term of Bessel function expansion of the potential solution.

In the calculations we have used a finite number of terms n (see the 6-th column) in the solution generated in such a way that we have a precision of W and F better than 10^{-3}.

The boundary conditions for the solution are:

$W(0,r) = 1500, \quad 0 \le r \le 2$

$W(1.5,r) = 0, \quad 0 \le r \le 2$

$W(z,2) = 0, \quad 0 < z \le 1.5$

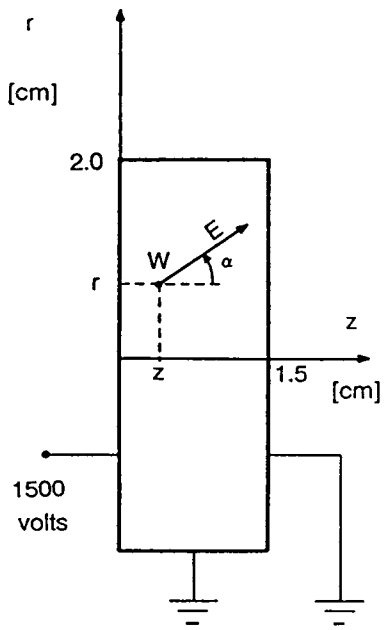

Data presented below show the potential W and the field F distribution for given points in space (z,r) in our experimental geometry. Basic advantage of these calculations is the proof that the field in the close vicinity of the axis of symmetry of the cylinder is almost uniform. We can see that for low values of r_i (below 4 mm) the values of α are low as well (below 4 deg.). This approximation for the field uniformity combined with the fact that the KrF excimer laser illuminates the center of the target give us sufficiently good foundations for simple model calculations of a trajectory parameters: times of flight t_f and t_o, radial deflection $r_f - r_i$ and the pulse values V_f and V_o. Results of these calculations are presented in Tables 2-5.

z [cm]	r [cm]	W [V]	F [V/cm]	α [deg]	n
0.15	0.20	0.13D+04	0.12D+04	0.54D+00	65
0.15	0.40	0.13D+04	0.12D+04	0.12D+01	65
0.15	0.60	0.13D+04	0.12D+04	0.19D+01	64
0.15	0.80	0.13D+04	0.13D+04	0.30D+01	63
0.15	1.00	0.13D+04	0.14D+04	0.44D+01	62
0.15	1.20	0.13D+04	0.16D+04	0.67D+01	61
0.15	1.40	0.12D+04	0.19D+04	0.10D+02	61
0.15	1.60	0.11D+04	0.25D+04	0.17D+02	61
0.15	1.80	0.85D+03	0.39D+04	0.34D+02	61
0.15	2.00	0.86D-12	0.60D+04	0.90D+02	61
0.30	0.20	0.12D+04	0.11D+04	0.10D+01	33
0.30	0.40	0.11D+04	0.11D+04	0.22D+01	33
0.30	0.60	0.11D+04	0.12D+04	0.37D+01	32
0.30	0.80	0.11D+04	0.12D+04	0.57D+01	32
0.30	1.00	0.11D+04	0.13D+04	0.85D+01	31
0.30	1.20	0.10D+04	0.15D+04	0.13D+02	31
0.30	1.40	0.95D+03	0.17D+04	0.19D+02	31
0.30	1.60	0.80D+03	0.20D+04	0.31D+02	31
0.30	1.80	0.50D+03	0.26D+04	0.52D+02	31
0.30	2.00	0.56D-12	0.28D+04	0.90D+02	31
0.45	0.20	0.99D+03	0.11D+04	0.14D+01	22
0.45	0.40	0.98D+03	0.11D+04	0.31D+01	22
0.45	0.60	0.96D+03	0.11D+04	0.51D+01	22
0.45	0.80	0.94D+03	0.12D+04	0.79D+01	21
0.45	1.00	0.90D+03	0.12D+04	0.12D+02	21
0.45	1.20	0.84D+03	0.13D+04	0.17D+02	21
0.45	1.40	0.74D+03	0.14D+04	0.26D+02	21
0.45	1.60	0.58D+03	0.16D+04	0.39D+02	21
0.45	1.80	0.33D+03	0.17D+04	0.60D+02	21
0.45	2.00	0.39D-12	0.17D+04	0.90D+02	21
0.60	0.20	0.83D+03	0.10D+04	0.17D+01	17
0.60	0.40	0.82D+03	0.11D+04	0.37D+01	17
0.60	0.60	0.80D+03	0.11D+04	0.61D+01	16
0.60	0.80	0.77D+03	0.11D+04	0.94D+01	16
0.60	1.00	0.73D+03	0.11D+04	0.14D+02	16
0.60	1.20	0.66D+03	0.11D+04	0.21D+02	16
0.60	1.40	0.56D+03	0.12D+04	0.30D+02	16
0.60	1.60	0.42D+03	0.12D+04	0.44D+02	16
0.60	1.80	0.23D+03	0.12D+04	0.64D+02	16
0.60	2.00	0.29D-12	0.11D+04	0.90D+02	16

0.75	0.20	0.68D+03	0.10D+04	0.18D+01	14
0.75	0.40	0.67D+03	0.10D+04	0.39D+01	13
0.75	0.60	0.65D+03	0.10D+04	0.66D+01	13
0.75	0.80	0.62D+03	0.99D+03	0.10D+02	13
0.75	1.00	0.58D+03	0.99D+03	0.15D+02	13
0.75	1.20	0.51D+03	0.98D+03	0.22D+02	13
0.75	1.40	0.43D+03	0.97D+03	0.32D+02	13
0.75	1.60	0.31D+03	0.93D+03	0.46D+02	13
0.75	1.80	0.16D+03	0.87D+03	0.65D+02	13
0.75	2.00	0.21D-12	0.79D+03	0.90D+02	13
0.90	0.20	0.53D+03	0.95D+03	0.18D+01	11
0.90	0.40	0.52D+03	0.94D+03	0.38D+01	11
0.90	0.60	0.50D+03	0.93D+03	0.64D+01	11
0.90	0.80	0.48D+03	0.91D+03	0.98D+01	11
0.90	1.00	0.44D+03	0.88D+03	0.15D+02	11
0.90	1.20	0.39D+03	0.84D+03	0.21D+02	11
0.90	1.40	0.32D+03	0.79D+03	0.31D+02	11
0.90	1.60	0.22D+03	0.71D+03	0.45D+02	11
0.90	1.80	0.11D+03	0.63D+03	0.65D+02	11
0.90	2.00	0.15D-12	0.56D+03	0.90D+02	11
1.05	0.20	0.39D+03	0.91D+03	0.16D+01	10
1.05	0.40	0.38D+03	0.90D+03	0.33D+01	10
1.05	0.60	0.37D+03	0.87D+03	0.56D+01	10
1.05	0.80	0.35D+03	0.84D+03	0.86D+01	9
1.05	1.00	0.32D+03	0.80D+03	0.13D+02	10
1.05	1.20	0.28D+03	0.73D+03	0.19D+02	10
1.05	1.40	0.22D+03	0.65D+03	0.28D+02	9
1.05	1.60	0.16D+03	0.55D+03	0.42D+02	9
1.05	1.80	0.79D+02	0.45D+03	0.62D+02	9
1.05	2.00	0.11D-12	0.38D+03	0.90D+02	9
1.20	0.20	0.26D+03	0.87D+03	0.11D+01	9
1.20	0.40	0.25D+03	0.86D+03	0.25D+01	9
1.20	0.60	0.24D+03	0.83D+03	0.41D+01	9
1.20	0.80	0.23D+03	0.79D+03	0.64D+01	8
1.20	1.00	0.21D+03	0.73D+03	0.96D+01	8
1.20	1.20	0.18D+03	0.65D+03	0.14D+02	8
1.20	1.40	0.14D+03	0.54D+03	0.22D+02	8
1.20	1.60	0.98D+02	0.43D+03	0.33D+02	8
1.20	1.80	0.50D+02	0.31D+03	0.54D+02	8
1.20	2.00	0.68D-13	0.24D+03	0.90D+02	8
1.35	0.20	0.13D+03	0.85D+03	0.61D+00	8
1.35	0.40	0.12D+03	0.84D+03	0.13D+01	8
1.35	0.60	0.12D+03	0.80D+03	0.22D+01	8
1.35	0.80	0.11D+03	0.76D+03	0.34D+01	8

1.35	1.00	0.10D+03	0.69D+03	0.52D+01	8
1.35	1.20	0.87D+02	0.60D+03	0.78D+01	7
1.35	1.40	0.69D+02	0.48D+03	0.12D+02	8
1.35	1.60	0.48D+02	0.34D+03	0.19D+02	7
1.35	1.80	0.24D+02	0.20D+03	0.37D+02	7
1.35	2.00	0.33D-13	0.12D+03	0.90D+02	7
1.50	0.20	-0.46D-31	0.85D+03	-0.33D-33	7
1.50	0.40	-0.44D-31	0.83D+03	-0.69D-33	7
1.50	0.60	-0.42D-31	0.79D+03	-0.11D-32	6
1.50	0.80	-0.38D-31	0.74D+03	-0.16D-32	7
1.50	1.00	-0.34D-31	0.67D+03	-0.22D-32	7
1.50	1.20	-0.28D-31	0.58D+03	-0.30D-32	7
1.50	1.40	-0.21D-31	0.46D+03	-0.43D-32	7
1.50	1.60	-0.14D-31	0.32D+03	-0.66D-32	7
1.50	1.80	-0.70D-32	0.16D+03	-0.13D-31	7
1.50	2.00	-0.94D-47	0.19D-12	-0.94D-17	1

```
c       THIS CODE SOLVES THE LAPLACE'S EQUATION IN A CYLINDER
c       AND CALCULATES POTENTIAL AND FIELD DISTRIBUTIONS
c                rad=radius of cylinder [cm]
c                hh =length of cylinder [cm]
c                jj =no. of blocks you want to devide radius
c                    ( there are calculations in jj+1 points )
c                kk =no. of blocks you want to devide length
c                v0 =constant potential on the top
c                v1 =constant potential on the bottom
c                  ( walls are always grounded )
c                apot=accuracy of potential
c                afiel=accuracy of field
c
c
         parameter (idimn=200)
         real*16 root(idimn),deriv(idimn)
         real*16 rad,v0,v1,al,err,f11,ezz,z,y,hh,ez,xn,
     *       yn,xn1,an,bn,eh,c,alr,f1,er,anc,bnc,fr,efr,
     *       egr,eee,t,tt,xx,r,ann,d11,apot,afiel,alhh,
     *       alz,er2,d00,bessj0,bessj1
         data rad/2.0Q0/,jj/10/,hh/1.5Q0/,kk/10/,v0/0.0Q0/,
     *        v1/1.5Q3/,apot/1.0Q-3/,afiel/1.0Q-3/
         call bessel(root,deriv,idimn)
c         do 9999 i=1,idimni]
c 9999   type 9961,i,root(i),deriv(i)
c 9961   format(4x,i3,3x,d29.20,3x,d29.20)
         type 11
   11    format(///5x,' (z,r)=coordinates of a point where
     *   potential and field are calculated'/
     *   5x,' angle is calculatad between a vector
     *    of field and axis of symmetry '/5x,' n=no. of terms
     *    in the series used to calculate a given potential'///)
         type 14
   14    format(8x,'z',15x,'r',11x,'pot',11x,'field',10x,
     *   'angle',8x,'n'/)
         do 100 k=2,kk+1
         z=hh*(k-1)/kk
         do 200 j=1,jj+1
         r=rad*(j-1)/jj
         n=0
         f11=0.0Q0
         err=0.0Q0
         ezz=0.0Q0
   20    n=n+1
         if(n.lt.idimn) go to 30
         type 12
   12    format(6x,'more roots needed ')
         go to 200
```

```
30    y=root(n)
      al=y/rad
      xn1=deriv(n)
      xx=2.0Q0/(y*xn1)
      xn=v1*xx
      yn=v0*xx
      alhh=al*hh
      if(alhh.gt.11350.0Q0) go to 200
      eh=qexp(alhh)
      ann=1.0Q0/(eh-1.0Q0/eh)
      an=ann*(yn-xn/eh)
      bn=ann*(xn*eh-yn)
      alz=al*z
      if(alz.gt.11350.0Q0) go to 200
      c=qexp(alz)
      alr=al*r
      if(alr.eq.0.0Q0) go to 200
      d00=bessj0(alr)
      d11=bessj1(alr)
      anc=an*c
      bnc=bn/c
      f1=(anc+bnc)*d00
      er=(anc+bnc)*d11*al
      ez=(bnc-anc)*d00*al
      f11=f11+f1
      err=err+er
      ezz=ezz+ez
      fr=qabs(f1)
      if(fr.gt.apot) go to 20
      efr=qabs(er)
      if(efr.gt.afiel) go to 20
      egr=qabs(ez)
      if(egr.gt.afiel) go to 20
      er2=err**2+ezz**2
      eee=qsqrt(er2)
      if(ezz.eq.0.0Q0) go to 40
      t=err/ezz
      tt=qatand(t)
      go to 50
40    if(err.gt.0.0Q0) go to 41
      if(err.lt.0.0Q0) go to 42
      tt=0.0Q0
      go to 50
41    tt=9.0Q1
      go to 50
42    tt=-9.0Q1
50    type 13,z,r,f11,eee,tt,n
```

```
  13    format(2x,2(f6.2,3x),3(d9.2,3x),i3)
 200    continue
 100    continue
        stop
        end

        subroutine bessel(root,deriv,idimn)
        real*16 root(idimn),deriv(idimn)
C
C
c       program calculates roots of Bessel function
c       of zeroth order and values of the first order
c       Bessel function at these points.
c       data to enter are:
c         step=step of searching for the roots
c         is=factor by which we want to change step
c         start=initial point where we want to start
c               the search
c         limit=final point where we want to stop the search
c         n1=starting position of a counter
c         prec=precision of roots of Bessel function J0
c              (max.error)
c
c
        real*16 step,start,h,x,y,sk1,sk2,sk3,sk,sk4,
     *          prec,bessj0,bessj1
        data n1/0/,step/1.0Q0/,is/2/,start/1.0Q0/,prec/1.0Q-15/
c        type 11
        jxx=1
c  11    format (///5x,'n        root',23x,'j1(root)'//)
        y=start
        n=n1
  20    h=step
        n=n+1
  10    x=y
  30    y=x+h
        sk1=bessj0(x)
        sk2=bessj0(y)
        sk=sk1*sk2
        if(sk.eq.0.0Q0) go to 40
        if(sk.gt.0.0Q0) go to 10
        if(h.lt.prec) go to 50
        h=h/2.0Q0
        go to 30
  40    sk3=bessj1(x)
        sk4=bessj1(y)
        type 41
```

```
  41    format(/3x,'for n= ',i3,'possible root '
     *         /15x,'  x   ,   y ',d19.10,3x,d19.10
     *         /15x,'j0(x),j1(y)',d19.10,3x,d19.10
     *         /15x,'j1(x),j1(y)',d19.10,3x,d19.10)
        go to 70
  50    sk3=bessj1(x)
  60    root(jxx)=x
        deriv(jxx)=sk3
        jxx=jxx+1
c        type 61,n,x,sk3
c  61    format(4x,i3,3x,d29.20,2x,d29.20)
        if(n.lt.idimn) go to 20
  70    return
        end

        real*16 function bessj0(x9)
        real*16 x9,h02,y,p1,p2,p3,p4,p5,q1,q2,q3,q4,q5,
     *    r1,r2,r3,r4,r5,r6,s1,s2,s3,s4,s5,s6,ax,z,xx,h01
        data p1,p2,p3,p4,p5/1.Q0,-.1098628627Q-2,.2734510407Q-4,
     *    -.2073370639Q-5,.2093887211Q-6/
        data q1,q2,q3,q4,q5/-.1562499995Q-1,.1430488765Q-3,
     *    -.6911147651Q-5,.7621095161Q-6,-.934945152Q-7/
        data r1,r2,r3,r4,r5,r6/57568490574.Q0,-13362590354.Q0,
     *    651619640.7Q0,-11214424.18Q0,77392.33017Q0,
     *    -184.9052456Q0/
        data s1,s2,s3,s4,s5,s6/57568490411.Q0,1029532985.Q0,
     *    9494680.718Q0,59272.64853Q0,267.8532712Q0,1.Q0/
        h01=8.0Q0
        h02=qabs(x9)
        if(h02.lt.h01) then
        y=x9**2
        bessj0=(r1+y*(r2+y*(r3+y*(r4+y*(r5+y*r6)))))
     *      /(s1+y*(s2+y*(s3+y*(s4+y*(s5+y*s6)))))
        else
        ax=qabs(x9)
        z=8.0Q0/ax
        y=z**2
        xx=ax-.78539816Q0
        bessj0=qsqrt(.636619772Q0/ax)*(qcos(xx)*(p1+y*(p2+y*
     *  (p3+y*(p4+y*p5))))-z*qsin(xx)*(q1+y*(q2+y*(q3+y*(q4+
     *  y*q5)))))
        endif
        return
        END
```

```
 real*16 function bessj1(x)
 real*16 y,p1,p2,p3,p4,p5,q1,q2,q3,q4,q5,r1,r2,r3,
*    r4,r5,r6,s1,s2,s3,s4,s5,s6,x,ax,z,xx
 data r1,r2,r3,r4,r5,r6/72362614232.Q0,-7895059235.Q0,
*    242396853.1Q0,-2972611.439Q0,15704.48260Q0,
*    -30.16036606Q0/,s1,s2,s3,s4,s5,s6/144725228442.Q0,
*    2300535178.Q0,18583304.74Q0,99447.43394Q0,
*    376.9991397Q0,1.Q0/
 data p1,p2,p3,p4,p5/1.Q0,.183105Q-2,-.3516396496Q-4,
*    .2457520174Q-5,-.240337019Q-6/, q1,q2,q3,q4,q5
*    /.04687499995Q0,-.2002690873Q-3,
*    .8449199096Q-5,-.88228987Q-6,.105787412Q-6/
 if(qabs(x).lt.8.0Q0)then
   y=x**2
   bessj1=x*(r1+y*(r2+y*(r3+y*(r4+y*(r5+y*r6)))))
*      /(s1+y*(s2+y*(s3+y*(s4+y*(s5+y*s6)))))
 else
   ax=qabs(x)
   z=8.0Q0/ax
   y=z**2
   xx=ax-2.35619491Q0
   bessj1=qsqrt(.636619772Q0/ax)*(qcos(xx)*(p1+y*
*   (p2+y*(p3+y*(p4+y*p5))))-z*qsin(xx)*(q1+y*(q2+
*   y*(q3+y*(q4+y*q5)))))*qsign(1.0Q0,x)
 endif
 return
 end
```

APPENDIX B

Potential W Distribution in a Cylindrical Box Obtained by Numerical Program FIELD

This program uses the relaxation method for finite differences with the following boundary conditions:

$W[0][j] = 1500, \quad 0 \le j \le 81$

$W[61][j] = 0, \quad 0 \le j \le 81$

$W[i][81] = 0, \quad 0 < i \le 61$

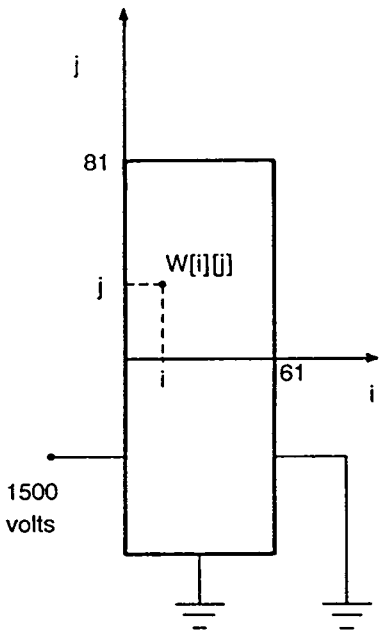

Potentials calculated here differ from the values calculated in the Appendix A by less then 2%. That indicates that our theoretical model is very accurate. Results of these calculations will be used for further calculations (Appendices C and E) of electrons and ions' trajectories. Note, that program FIELD has very powerful capabilities for finding electrostatic fields in different geometries. We can use it in more complicated cases when electrodes of a different shape are inserted inside.

```
THE FOLLOWING CALCULATION OF ELECTROSTATIC POTENTIAL IS FOR:
ff


THE FOLLOWING CALCULATION OF ELECTROSTATIC POTENTIAL IS FOR:
q

Vertical reflection symmetry.


rlen =     15.000  nxm = 61   nym = 81


Top line segment number 0
xl = 0.000000, wl = 0.000010, x2 = 15.000000, w2 = 0.000010

Left end potential = 1500.000000

Right end potential = 0.000010

THE FOLLOWING CALCULATION OF ELECTROSTATIC POTENTIAL IS FOR:
rrr

Vertical reflection symmetry.


rlen =     15.000  nxm = 61   nym = 81


Top line segment number 0
xl = 0.000000, wl = 0.001000, x2 = 15.000000, w2 = 0.001000

Left end potential = 1500.000000

Right end potential = 0.001000
Maximum number of initial iterations = 300

Cyllindrical geometry.

Time for refining = 591 sec for 301 iterations.


ic[0] = 0

iyl[0][0] = 0

w[0][0] = 1500.00000
w[0][8] = 1500.00000   w[0][16] = 1500.00000   w[0][24] = 1500.00000
w[0][32] = 1500.00000   w[0][40] = 1500.00000   w[0][48] = 1500.00000
w[0][56] = 1500.00000   w[0][64] = 1500.00000   w[0][72] = 1500.00000
w[0][80] = 1500.00000

ic[6] = 1

iyl[0][6] = 1
iyl[1][6] = 79
```

```
w[6][0] = 1336.97852
w[6][8] = 1335.98376   w[6][16] = 1332.90796   w[6][24] = 1327.04114
w[6][32] = 1316.99719   w[6][40] = 1300.18018   w[6][48] = 1271.52954
w[6][56] = 1220.02856   w[6][64] = 1116.20325   w[6][72] =  851.16003
w[6][80] =    0.00100

ic[12] = 1

iyl[0][12] = 1
iyl[1][12] = 79

w[12][0] = 1175.28931
w[12][8] = 1173.41553   w[12][16] = 1167.63733   w[12][24] = 1156.67090
w[12][32] = 1138.05530   w[12][40] = 1107.33032   w[12][48] = 1056.29358
w[12][56] =  968.93805   w[12][64] =  811.09625   w[12][72] =  509.45532
w[12][80] =    0.00100

ic[18] = 1

iyl[0][18] = 1
iyl[1][18] = 79

w[18][0] = 1016.14832
w[18][8] = 1013.61090   w[18][16] = 1005.81610   w[18][24] =  991.13055
w[18][32] =  966.50958   w[18][40] =  926.69690   w[18][48] =  862.81049
w[18][56] =  759.95184   w[18][64] =  594.19080   w[18][72] =  336.94849
w[18][80] =    0.00100

ic[24] = 1

iyl[0][24] = 1
iyl[1][24] = 79

w[24][0] =  860.45636
w[24][8] =  857.53497   w[24][16] =  848.60150   w[24][24] =  831.91693
w[24][32] =  804.34778   w[24][40] =  760.79047   w[24][48] =  693.43103
w[24][56] =  591.22382   w[24][64] =  441.25494   w[24][72] =  237.18463
w[24][80] =    0.00100

ic[30] = 1

iyl[0][30] = 1
iyl[1][30] = 79

w[30][0] =  708.71484
w[30][8] =  705.71362   w[30][16] =  696.57916   w[30][24] =  679.67328
w[30][32] =  652.14966   w[30][40] =  609.64813   w[30][48] =  546.14301
w[30][56] =  454.51236   w[30][64] =  329.07599   w[30][72] =  171.74751
w[30][80] =    0.00100

ic[36] = 1

iyl[0][36] = 1
iyl[1][36] = 79

w[36][0] =  561.00610
w[36][8] =  558.21686   w[36][16] =  549.76544   w[36][24] =  534.25653
w[36][32] =  509.34946   w[36][40] =  471.66455   w[36][48] =  416.96927
w[36][56] =  341.09476   w[36][64] =  242.17889   w[36][72] =  124.26182
```

```
w[36][80] =    0.00100

ic[42] = 1

iyl[0][42] = 1
iyl[1][42] = 79

w[42][0] =  417.02478
w[42][8] =  414.70041   w[42][16] =  407.68451   w[42][24] =  394.90286
w[42][32] =  374.60922   w[42][40] =  344.40955   w[42][48] =  301.55905
w[42][56] =  243.80460   w[42][64] =  170.96362   w[42][72] =   86.84064
w[42][80] =    0.00100

ic[48] = 1

iyl[0][48] = 1
iyl[1][48] = 79

w[48][0] =  276.14127
w[48][8] =  274.47928   w[48][16] =  269.47745   w[48][24] =  260.41510
w[48][32] =  246.14928   w[48][40] =  225.17575   w[48][48] =  195.88902
w[48][56] =  157.17845   w[48][64] =  109.38133   w[48][72] =   55.23249
w[48][80] =    0.00100

ic[54] = 1

iyl[0][54] = 1
iyl[1][54] = 79

w[54][0] =  137.48007
w[54][8] =  136.61484   w[54][16] =  134.01566   w[54][24] =  129.32280
w[54][32] =  121.97454   w[54][40] =  111.25096   w[54][48] =   96.41962
w[54][56] =   77.03679   w[54][64] =   53.38776   w[54][72] =   26.87406
w[54][80] =    0.00100

ic[60] = 0

iyl[0][60] = 0

w[60][0] =    0.00100
w[60][8] =    0.00100   w[60][16] =    0.00100   w[60][24] =    0.00100
w[60][32] =    0.00100   w[60][40] =    0.00100   w[60][48] =    0.00100
w[60][56] =    0.00100   w[60][64] =    0.00100   w[60][72] =    0.00100
w[60][80] =    0.00100

filename for potential = ut
```

APPENDIX C

Sample Results of Trajectory Calculations by Program TRAJS for Charged Particles Emitted into Accelerating Field F in Direction of Force

Potentials for these trajectories were calculated by the program FIELD; for details see the Appendix B. Times of flight for e^-, Si^+, Ge^+ ejected into the field along the force vector with different initial energies, at different initial angles to the axes of symmetry and the corresponding results of analytical calculations are presented in Tables 2-4.

```
Potential file name = ut

Charge of ion = 1.000000

Mass of ion in amu = 0.000549

Mean energy = 1500.000000

alpha = 1.000000


Equipotentials to be plotted:

potential[1] = 1.000000
potential[2] = 10.000000
potential[3] = 100.000000
potential[4] = 500.000000
potential[5] = 800.000000
potential[6] = 1200.000000
potential[7] = 1400.000000
potential[8] = 1450.000000
potential[9] = 1470.000000
potential[10] = 1490.000000

SUMMARY FOR THIS TRAJECTORY:

INIT VX = 18.747551 mm/micsec  INIT VY = 0.000000 mm/micsec
FLIGHT TIME = 0.001241 micsec  FIN. POS.: x = 14.689456 mm y = 0.546412 mm
INITIAL X = 0.250000 mm  INITIAL Y = 0.500000 mm
INITIAL ANGLE REL. X-AXIS = 0.000000 radians
 Final vy/vx = 0.004310
INITIAL ENERGY = 0.001000 eV.
KINETIC ENERGY at 14.567267,0.545885 = 1433.311035 eV.


SUMMARY FOR THIS TRAJECTORY:

INIT VX = 593.149780 mm/micsec  INIT VY = 0.000000 mm/micsec
FLIGHT TIME = 0.001219 micsec  FIN. POS.: x = 14.867677 mm y = 0.546781 mm
INITIAL X = 0.250000 mm  INITIAL Y = 0.500000 mm
INITIAL ANGLE REL. X-AXIS = 0.000000 radians
 Final vy/vx = 0.004273
INITIAL ENERGY = 1.001000 eV.
KINETIC ENERGY at 14.744755,0.546256 = 1450.578857 eV.


SUMMARY FOR THIS TRAJECTORY:

INIT VX = 838.630920 mm/micsec  INIT VY = 0.000000 mm/micsec
FLIGHT TIME = 0.001209 micsec  FIN. POS.: x = 14.903425 mm y = 0.546663 mm
INITIAL X = 0.250000 mm  INITIAL Y = 0.500000 mm
INITIAL ANGLE REL. X-AXIS = 0.000000 radians
 Final vy/vx = 0.004256
INITIAL ENERGY = 2.001000 eV.
KINETIC ENERGY at 14.780323,0.546139 = 1454.813354 eV.
```

Potential file name = ut

Charge of ion = 1.000000

Mass of ion in amu = 28.086000

Mean energy = 1500.000000

alpha = 1.000000

SUMMARY FOR THIS TRAJECTORY:

INIT VX = 0.082887 mm/micsec INIT VY = 0.000000 mm/micsec
FLIGHT TIME = 0.280744 micsec FIN. POS.: x = 14.689456 mm y = 0.546412 mm
INITIAL X = 0.250000 mm INITIAL Y = 0.500000 mm
INITIAL ANGLE REL. X-AXIS = 0.000000 radians
Final vy/vx = 0.004310
INITIAL ENERGY = 0.001000 eV.
KINETIC ENERGY at 14.567267,0.545885 = 1433.311157 eV.

SUMMARY FOR THIS TRAJECTORY:

INIT VX = 2.622440 mm/micsec INIT VY = 0.000000 mm/micsec
FLIGHT TIME = 0.275819 micsec FIN. POS.: x = 14.867677 mm y = 0.546781 mm
INITIAL X = 0.250000 mm INITIAL Y = 0.500000 mm
INITIAL ANGLE REL. X-AXIS = 0.000000 radians
Final vy/vx = 0.004273
INITIAL ENERGY = 1.001000 eV.
KINETIC ENERGY at 14.744755,0.546256 = 1450.579102 eV.

SUMMARY FOR THIS TRAJECTORY:

INIT VX = 3.707764 mm/micsec INIT VY = 0.000000 mm/micsec
FLIGHT TIME = 0.273356 micsec FIN. POS.: x = 14.903425 mm y = 0.546663 mm
INITIAL X = 0.250000 mm INITIAL Y = 0.500000 mm
INITIAL ANGLE REL. X-AXIS = 0.000000 radians
Final vy/vx = 0.004256
INITIAL ENERGY = 2.001000 eV.
KINETIC ENERGY at 14.780323,0.546139 = 1454.813477 eV.

SUMMARY FOR THIS TRAJECTORY:

INIT VX = 4.540687 mm/micsec INIT VY = 0.000000 mm/micsec
FLIGHT TIME = 0.270894 micsec FIN. POS.: x = 14.871510 mm y = 0.546362 mm
INITIAL X = 0.250000 mm INITIAL Y = 0.500000 mm
INITIAL ANGLE REL. X-AXIS = 0.000000 radians
Final vy/vx = 0.004251
INITIAL ENERGY = 3.001000 eV.
KINETIC ENERGY at 14.748489,0.545839 = 1452.898071 eV.

SUMMARY FOR THIS TRAJECTORY:

Potential file name = ut

Charge of ion = 1.000000

Mass of ion in amu = 72.589897

Mean energy = 1500.000000

alpha = 1.000000

SUMMARY FOR THIS TRAJECTORY:

INIT VX = 0.051558 mm/micsec INIT VY = 0.000000 mm/micsec
FLIGHT TIME = 0.451340 micsec FIN. POS.: x = 14.689456 mm y = 0.546412 mm
INITIAL X = 0.250000 mm INITIAL Y = 0.500000 mm
INITIAL ANGLE REL. X-AXIS = 0.000000 radians
 Final vy/vx = 0.004310
INITIAL ENERGY = 0.001000 eV.
KINETIC ENERGY at 14.567267,0.545885 = 1433.311157 eV.

SUMMARY FOR THIS TRAJECTORY:

INIT VX = 1.631220 mm/micsec INIT VY = 0.000000 mm/micsec
FLIGHT TIME = 0.443421 micsec FIN. POS.: x = 14.867677 mm y = 0.546781 mm
INITIAL X = 0.250000 mm INITIAL Y = 0.500000 mm
INITIAL ANGLE REL. X-AXIS = 0.000000 radians
 Final vy/vx = 0.004273
INITIAL ENERGY = 1.001000 eV.
KINETIC ENERGY at 14.744755,0.546256 = 1450.579102 eV.

SUMMARY FOR THIS TRAJECTORY:

INIT VX = 2.306317 mm/micsec INIT VY = 0.000000 mm/micsec
FLIGHT TIME = 0.439462 micsec FIN. POS.: x = 14.903425 mm y = 0.546663 mm
INITIAL X = 0.250000 mm INITIAL Y = 0.500000 mm
INITIAL ANGLE REL. X-AXIS = 0.000000 radians
 Final vy/vx = 0.004256
INITIAL ENERGY = 2.001000 eV.
KINETIC ENERGY at 14.780323,0.546139 = 1454.813354 eV.

SUMMARY FOR THIS TRAJECTORY:

INIT VX = 2.824414 mm/micsec INIT VY = 0.000000 mm/micsec
FLIGHT TIME = 0.435503 micsec FIN. POS.: x = 14.871510 mm y = 0.546362 mm
INITIAL X = 0.250000 mm INITIAL Y = 0.500000 mm
INITIAL ANGLE REL. X-AXIS = 0.000000 radians
 Final vy/vx = 0.004251
INITIAL ENERGY = 3.001000 eV.
KINETIC ENERGY at 14.748489,0.545839 = 1452.897949 eV.

SUMMARY FOR THIS TRAJECTORY:

APPENDIX D

Sample Results of Analytical Calculations of the Final Time of Flight for Charges Accelerated in a Uniform Electrostatic Field

The values of the final time of flight (t_f) for e^-, Ge^+, Si^+ were calculated analytically using the eq. (6). These results show the relationship between initial velocities and the flight time in different, uniform electrostatic fields. For the selected values of initial velocity these data were plotted on the graphs as a function of bias voltage, $t_f = f(V_1)$, and presented in the Figs. 21-23. Note, that for very high velocities we do not make corrections for relativistic effects. It is highly improbable to achieve these values in our experiment.

V_1 [volts]	F [volts/mm]	v_o [m/s]	t_f [ns]
for electrons			
0.150D+04	0.100D+03	0.100D+02	0.131D+01
0.150D+04	0.100D+03	0.200D+03	0.131D+01
0.150D+04	0.100D+03	0.300D+04	0.131D+01
0.150D+04	0.100D+03	0.400D+05	0.130D+01
0.150D+04	0.100D+03	0.500D+06	0.128D+01
0.150D+04	0.100D+03	0.600D+07	0.101D+01
0.150D+04	0.100D+03	0.700D+08	0.209D+00
for Si+ ions			
0.150D+04	0.100D+03	0.100D+02	0.295D+03
0.150D+04	0.100D+03	0.200D+03	0.294D+03
0.150D+04	0.100D+03	0.300D+04	0.286D+03
0.150D+04	0.100D+03	0.400D+05	0.201D+03
0.150D+04	0.100D+03	0.500D+06	0.297D+02
0.150D+04	0.100D+03	0.600D+07	0.250D+01
0.150D+04	0.100D+03	0.700D+08	0.214D+00
for Ge+ ions			
0.150D+04	0.100D+03	0.100D+02	0.473D+03
0.150D+04	0.100D+03	0.200D+03	0.472D+03
0.150D+04	0.100D+03	0.300D+04	0.451D+03
0.150D+04	0.100D+03	0.400D+05	0.261D+03
0.150D+04	0.100D+03	0.500D+06	0.299D+02
0.150D+04	0.100D+03	0.600D+07	0.250D+01
0.150D+04	0.100D+03	0.700D+08	0.214D+00

```
c     THIS CODE CALCULATES THE TIME OF FLIGHT OF IONS OF
c     MASS M IN UNIFORM ELECTROSTATIC FIELD F TRAVELING
c     A DISTANCE H WITH DIFFERENT INITIAL VELOCITIES V0

          real*8 m,v0,ek0,h,v1,
     *         q,l,g,r,tfin,v0i
     *         z,dv1,v1f,dv0,v0f,v11
         integer qa,rr
         data m/54.9D-5/,v0/.1D-1/,ek0/0.D0/,h/15.D0/,qa/1/,
     *         v1/1.0D-5/,dv1/1.5d3/,v1f/1.5d3/,dv0/1.0d3/,
     *         v0f/1.0d9/
         q=qa*1.6021892D0
c  initial velocity never = 0
c         type 300 ,h
c  300    format(//3x,'for uniformly accelerated ions of mass m'
c     *  /3x,'in electrostatic field V/h  { h= ',
c     *   d10.3,' [mm] }'/
c     *  3x,'with initial velocity V0 '
c     *  ///3x,'V [V]',7x,'V/h [V/mm]',4x,'V0 [m/s]',
c     *  5x,'fin.time [ns]'/)
   501   v1=v1+dv1
         do 502 ii=1,7
         v0i=v0+ii*(1.0d1)**(ii)
         if (v0i.lt.ek0) go to 100
         l=v0i
         go to 200
   100   l=dsqrt(2.*ek0*1.6021892D8/(m*1.6605655D0))
   200   z=q*1.0D8/(m*1.6605655D0)
         g=l*h*m*1.6605655D-2/(q*v1)
         r=2.D0*z*v1/l**2+1.0D0
         tfin=g*(dsqrt(r)-1.0Q0)
         v11=v1/h
         type 301,v1,v11,v0i,tfin
   301   format(3x,4(d10.3,3x))
   502   continue
         if(v1.lt.v1f) go to 501
         stop
         end
```

APPENDIX E

Sample Results of Trajectory Calculations by Program TRAJS for Charged Particles Emitted into the Electrostatic Field F Against the Force

Program procedures are the same as in Appendix C; we simply change sign of the bias or sign of the particle.

The values of the field, created in our experiment by the bias voltage of 1500 volts, were calculated by the program FIELD, for details see Appendix B. Selected data on the particle deflection, $r_f - r_i$, and the total time of flight, $2t_o$, for different initial kinetic energies, are presented in Table 5.

bb

Potential file name = ut

Charge of ion = -1.000000

Mass of ion in amu = 0.000549

Mean energy = 1500.000000

alpha = 1.000000

SUMMARY FOR THIS TRAJECTORY:

INIT VX = 12576.320313 mm/micsec INIT VY = 0.000000 mm/micsec
FLIGHT TIME = 0.001350 micsec FIN. POS.: x = 0.123300 mm y = 0.424134 mm
INITIAL X = 0.250000 mm INITIAL Y = 0.500000 mm
INITIAL ANGLE REL. X-AXIS = 0.000000 radians
Final vy/vx = 0.008695
INITIAL ENERGY = 450.000000 eV.
KINETIC ENERGY at 0.192238,0.424734 = 456.267700 eV.

SUMMARY FOR THIS TRAJECTORY:

INIT VX = 18272.970703 mm/micsec INIT VY = 0.000000 mm/micsec
FLIGHT TIME = 0.002058 micsec FIN. POS.: x = 0.093000 mm y = 0.263398 mm
INITIAL X = 0.250000 mm INITIAL Y = 0.500000 mm
INITIAL ANGLE REL. X-AXIS = 0.000000 radians
Final vy/vx = 0.012299
INITIAL ENERGY = 950.000000 eV.
KINETIC ENERGY at 0.192795,0.264625 = 956.212097 eV.

SUMMARY FOR THIS TRAJECTORY:

INIT VX = 22575.185547 mm/micsec INIT VY = 0.000000 mm/micsec
FLIGHT TIME = 0.002657 micsec FIN. POS.: x = 0.219062 mm y = 0.246951 mm
INITIAL X = 0.250000 mm INITIAL Y = 0.500000 mm
INITIAL ANGLE REL. X-AXIS = 0.000000 radians
Final vy/vx = 0.008194
INITIAL ENERGY = 1450.000000 eV.
KINETIC ENERGY at 0.341533,0.247954 = 1440.016724 eV.

```
Potential file name = ut

Charge of ion = -1.000000

Mass of ion in amu = 28.086000

Mean energy = 1500.000000

alpha = 1.000000


SUMMARY FOR THIS TRAJECTORY:

INIT VX = 55.602566 mm/micsec  INIT VY = 0.000000 mm/micsec
FLIGHT TIME = 0.305371 micsec  FIN. POS.: x = 0.123300 mm y = 0.424134 mm
INITIAL X = 0.250000 mm  INITIAL Y = 0.500000 mm
INITIAL ANGLE REL. X-AXIS = 0.000000 radians
 Final vy/vx = 0.008695
INITIAL ENERGY = 450.000000 eV.
KINETIC ENERGY at 0.192238,0.424734 = 456.267761 eV.


SUMMARY FOR THIS TRAJECTORY:

INIT VX = 80.788651 mm/micsec  INIT VY = 0.000000 mm/micsec
FLIGHT TIME = 0.465443 micsec  FIN. POS.: x = 0.093000 mm y = 0.263398 mm
INITIAL X = 0.250000 mm  INITIAL Y = 0.500000 mm
INITIAL ANGLE REL. X-AXIS = 0.000000 radians
 Final vy/vx = 0.012299
INITIAL ENERGY = 950.000000 eV.
KINETIC ENERGY at 0.192795,0.264625 = 956.212341 eV.


SUMMARY FOR THIS TRAJECTORY:

INIT VX = 99.809654 mm/micsec  INIT VY = 0.000000 mm/micsec
FLIGHT TIME = 0.600891 micsec  FIN. POS.: x = 0.219050 mm y = 0.246951 mm
INITIAL X = 0.250000 mm  INITIAL Y = 0.500000 mm
INITIAL ANGLE REL. X-AXIS = 0.000000 radians
 Final vy/vx = 0.008194
INITIAL ENERGY = 1450.000000 eV.
KINETIC ENERGY at 0.341521,0.247954 = 1440.016968 eV.
```

Potential file name = ut

Charge of ion = -1.000000

Mass of ion in amu = 72.589897

Mean energy = 1500.000000

alpha = 1.000000

SUMMARY FOR THIS TRAJECTORY:

INIT VX = 34.586105 mm/micsec INIT VY = 0.000000 mm/micsec
FLIGHT TIME = 0.490931 micsec FIN. POS.: x = 0.123300 mm y = 0.424134 mm
INITIAL X = 0.250000 mm INITIAL Y = 0.500000 mm
INITIAL ANGLE REL. X-AXIS = 0.000000 radians
 Final vy/vx = 0.008695
INITIAL ENERGY = 450.000000 eV.
KINETIC ENERGY at 0.192238,0.424734 = 456.267761 eV.

SUMMARY FOR THIS TRAJECTORY:

INIT VX = 50.252449 mm/micsec INIT VY = 0.000000 mm/micsec
FLIGHT TIME = 0.748274 micsec FIN. POS.: x = 0.093000 mm y = 0.263398 mm
INITIAL X = 0.250000 mm INITIAL Y = 0.500000 mm
INITIAL ANGLE REL. X-AXIS = 0.000000 radians
 Final vy/vx = 0.012299
INITIAL ENERGY = 950.000000 eV.
KINETIC ENERGY at 0.192795,0.264625 = 956.212280 eV.

SUMMARY FOR THIS TRAJECTORY:

INIT VX = 62.083961 mm/micsec INIT VY = 0.000000 mm/micsec
FLIGHT TIME = 0.966025 micsec FIN. POS.: x = 0.219062 mm y = 0.246951 mm
INITIAL X = 0.250000 mm INITIAL Y = 0.500000 mm
INITIAL ANGLE REL. X-AXIS = 0.000000 radians
 Final vy/vx = 0.008194
INITIAL ENERGY = 1450.000000 eV.
KINETIC ENERGY at 0.341533,0.247954 = 1440.016846 eV.

VITAE

MIROSLAW MAREK BIALKOWSKI was born on May 23, 1955, in Lodz, Poland. He attended public elementary and high schools in Lodz and in 1979 completed his higher education at the Technical University of Lodz with the M.E. degree in Engineering Physics. His thesis, entitled "Research on the Usefulness of Silicon Transistors in Low Temperature Thermometry," was based on a research done partially in the Polish Academy of Sciences' Institute of Low Temperatures and Structural Research in Wroclaw, Poland.

On March 6, 1984 he came to the Department of Physics at the University of Tennessee, Knoxville, to continue his education. In December 1986 he met Dr. G. Samuel Hurst, his major research advisor, and became involved in Resonance Ionization Spectroscopy. This involvement led to work on a Small Business Innovative Research project for Pellissippi International, Inc., of Knoxville, Tennessee. That work has been presented in this thesis.